



EUROPEAN
COMMISSION

Community research

BELBaR

(Contract Number: 295487)

DELIVERABLE D2.11

WP2 partners final report on bentonite erosion

B+TECH: T. Schatz, R. Eriksson

Clay Technology AB: E. Ekvy Hansen, M. Hedström

CIEMAT: T. Missana, U.Alonso, N. Mayordomo, A.M. Fernández

KIT-INE: M. Bouby, S. Heck, F. Geyer, T. Schäfer

Date of issue of this report: 28/12/2015

Start date of project: 01/03/12

Duration: 48 Months

Project co-funded by the European Commission under the Seventh Euratom Framework Programme for Nuclear Research & Training Activities (2007-2011)		
Dissemination Level		
PU	Public	X
RE	Restricted to a group specified by the partners of the BELBaR project	
CO	Confidential, only for partners of the BELBaR project	

BELBaR



DISTRIBUTION LIST

Name	Number of copies	Comments
Christophe Davies (EC) BELBaR participants		

INTRODUCTION

The mechanisms of bentonite erosion from the compacted bentonite barrier of a high-level waste repository (HLWR), leading to the generation of (colloidal) particles detaching from the clay, are being deeply investigated in the EC-BELBAR Project. Two main reasons drive the interest of this study: the first concerns the integrity of the barrier at the long-term, which will be compromised if a significant clay loss occurs; the second one is about the role that clay colloids may play on radionuclide transport if they are stable and mobile in groundwater.

In EC-BELBaR Work Package 2 (WP2, “*Erosion*”), several research groups collaborated to identify the most important mechanisms involved in bentonite erosion and to quantify its possible extent under different environmental conditions.

Different possible scenarios were considered: the *static system*, where the transformation of the hydrated bentonite gel to a sol is mainly a chemically driven process and the *dynamic* one where other hydraulic aspects, as water velocity or fracture geometry must be considered. In fact, the worst scenario for a HLRW repository in crystalline rocks includes the presence of hydraulically active fractures near the bentonite surface.

In both scenarios, the extent of erosion is expected to depend mainly on the combination of water chemistry and clay properties; however, in the dynamic system, the water flowing at the bentonite surface (the gel-front) may increase colloid detachment.

Participated to WP2, eleven research organization from seven different countries: CIEMAT (Spain); MSU (Russia); KIT-INE (Germany); UJV-REZ (Czech Republic); SKB, ClayTech, KTH (Sweden); B+Tech, VTT, University of Jyväskylä (Finland); NDA (United Kingdom).

The objective of the present Deliverable 2.12 (“*WP2 partners final report on bentonite erosion*”) is to provide a summary of the main results obtained at the different research organization during the BELBaR Project in respect to the expected outcomes from WP2 to WP1. In particular: 1) mechanisms of clay colloid release; 2) the role of clay composition; 3) the role of groundwater chemistry; 4) the analysis of the dependence between the groundwater velocity and erosion rate; 5) the effect of fracture geometry on clay mass loss and 6) maximum clay mass loss rate.

Apart from the summary of results from the different organisations, this report will include an Annex in which the erosion rates estimated under different conditions will be provided as quantitative parameter to be fed in predictive models.

In order to address the goals of this WP, different experimental sets-up were used by the different organisations. Most of the tests were carried out simulating the potential extrusion/erosion behaviour of bentonite buffer material at a transmissive fracture interface (B+Tech; Clay Technology; CIEMAT). A schematic of this type of test can be seen in Figure 1 (from B+Tech). With this system, the effect of solution chemistry, material composition, flow velocity, fracture geometry (aperture, slope angle) and other parameters could be analysed. In this set-up, the swelling clay material can extrude/erode into an artificial fracture and it was selected for performing the tests of the benchmark exercise, also carried out in WP2.

Other types of experiments were carried out, maintaining the confinement of the clay and allowing its hydration through the presence of sintered steel filters with cells similar to those presented in Figure 2 (CIEMAT).

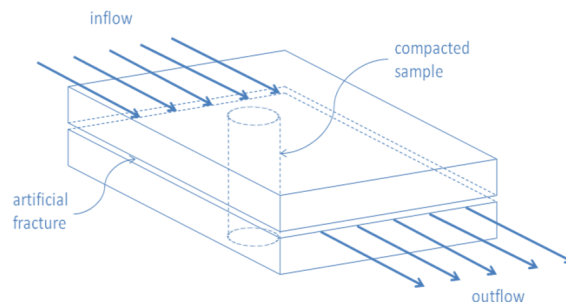


Figure 1. Schematic representation of the flow-through, artificial fracture test

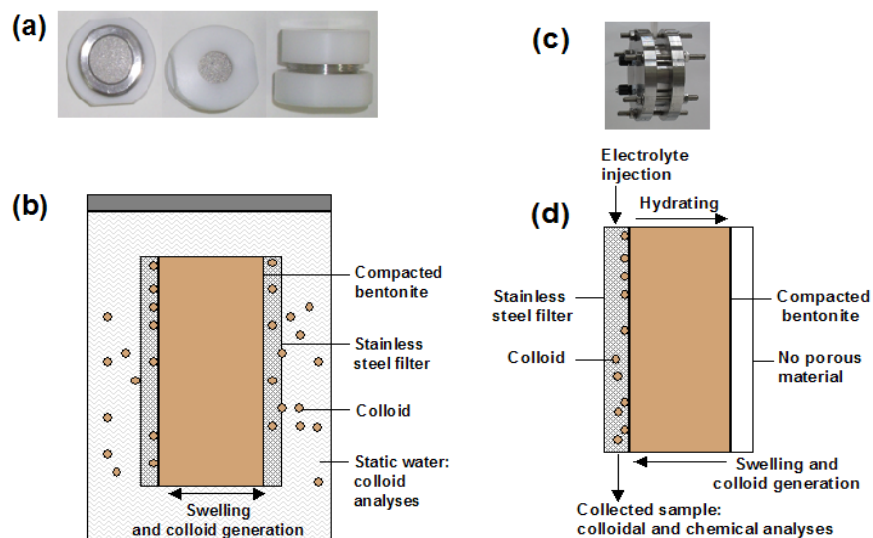


Figure 2. Schematic representation of erosion tests with confined clay a and b) static; and c and d) dynamic tests (CIEMAT).

These tests could represent *static conditions* (closed system with water in equilibrium with the clay, Figure 2a and 2b) or *dynamic conditions* (with water flowing at the surface of the bentonite, Figure 2c and 2d).

To analyse the results obtained from the different organisations and to be sure that the data provided in the Annex are comparable, is important to make clear how the “*mass loss*” or the “*average mass loss rate*”, needed for quantitatively estimating erosion, is measured in each case.

When the clay is confined, with no significant extrusion, the mass loss is limited to the particles dispersed in the liquid phase (or *eluted mass*) plus some particles retained in the sintered filters, which can be determined by difference from the initial and final weight of the initially *emplaced* mass.

In the artificial fracture tests, the mass loss is determined via post-mortem analysis considering also the material extruded in the fracture.

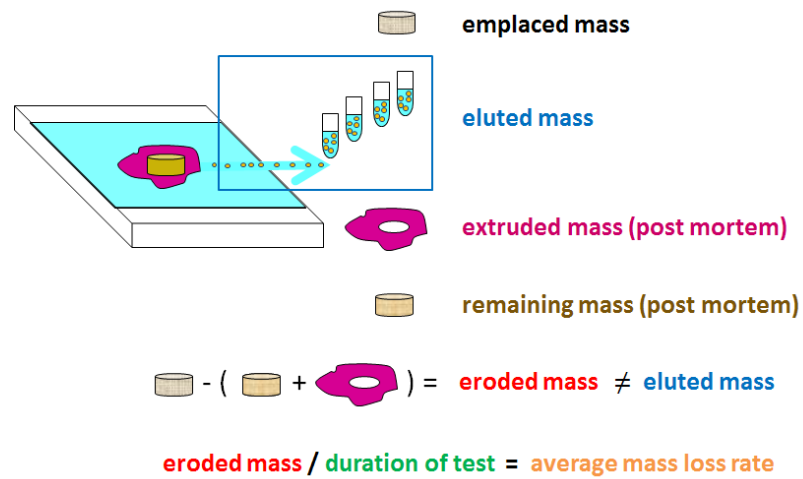


Figure 3. *Determination of the clay eroded mass in erosion tests.*

The nomenclature and the methodology of used to determine the eroded mass is schematized in Figure 3.

In the next Chapters, the detailed contributions of the different partners to the Deliverable 2.11 will be described.

CONTRIBUTION OF PARTNERS TO DELIVERABLE 2.11

1) SUMMARY OF MAIN RESULTS FOR WP2 OBTAINED AT B+TECH

Introduction

This report provides a summary of the main results obtained at B+Tech during the BELBaR Project with respect to the sought-after outcomes from WP2 to WP1. Specifically these outcomes are: 1) mechanisms of clay colloid release, 2) the role of divalent cations (clay composition), 3) the effect of mixed monovalent/divalent systems (groundwater chemistry), 4) verification of the dependence between the groundwater velocity and erosion rate, 5) the effect of fracture geometry on clay mass loss and 6) maximum clay mass loss rate.

Artificial Fracture Tests

In order to try to address the WP2 goals, small-scale, flow-through, artificial fracture tests, in which swelling clay material can extrude/erode into a well-defined, intersecting fracture (see Figure 4), were conducted at B+Tech. These experiments are performed in order to simulate the potential extrusion/erosion behaviour of bentonite buffer material at a transmissive fracture interface. Using such systems the effect of solution chemistry (salt concentration and composition), material composition (sodium montmorillonite and admixtures with calcium montmorillonite, natural bentonites), flow velocity, fracture geometry (aperture, slope angle) and the role of accessory minerals on erosion processes can be analysed. In principle artificial fractures tests can be used to support the determination of the erosive mass loss mechanism (outcomes 1 and 6) and demonstrate expectations with respect to outcomes 2 through 5.

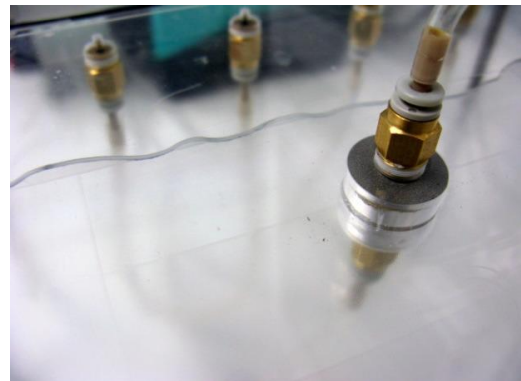
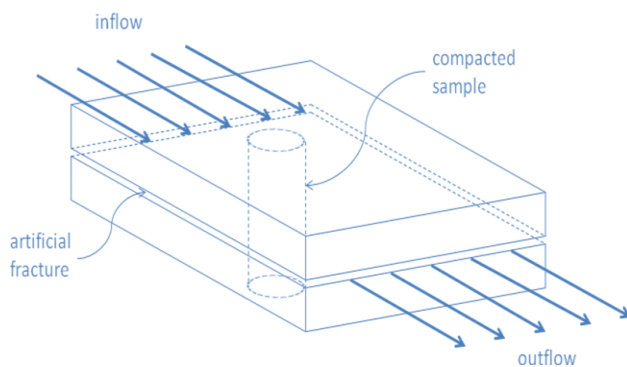


Figure 4. Schematic representation of the flow-through, artificial fracture test system design basis (left) and photographic image of a flow front approaching a compacted sampled through a 1 mm aperture, horizontal fracture (right).

At B+Tech, mass loss from artificial fracture tests is determined via post-mortem analysis (see Figure 5). Although effluent mass data is collected, due to the aggregation and sedimentation of eroding material (see B+Tech contribution to rheological studies), it does

not represent total eroding mass. As all liberated mass cannot be accounted for on the basis of collected effluent mass, erosion rates determined on this basis do not represent the full extent of mass loss. It can also be questioned whether extruded mass should be considered lost mass as it would no longer be contributing to buffer performance in the deposition hole per se, however, extruded material can serve an extended diffusive barrier function around the intersecting fracture/buffer interface. In any case, for the purposes of the following discussion, extruded material is not calculated as lost mass.

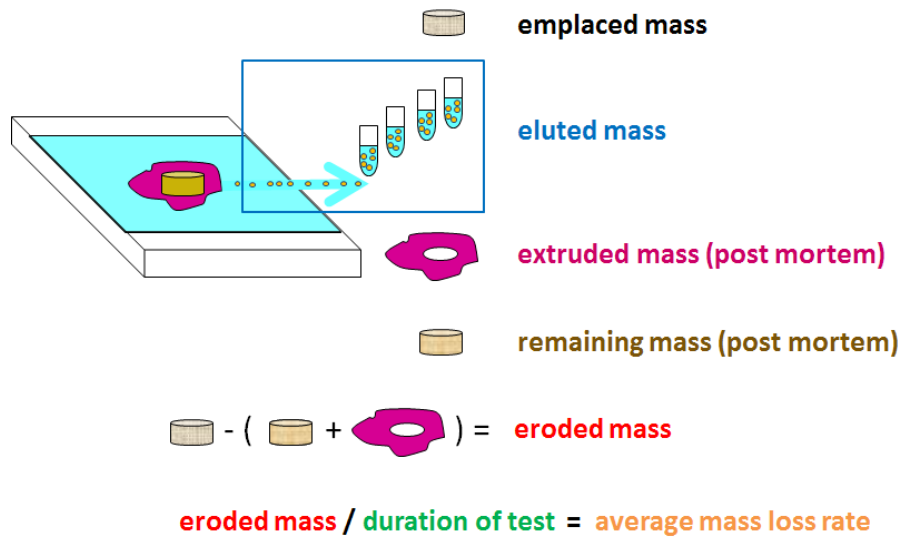


Figure 5. *Illustration of artificial fracture test mass loss analysis (adapted from graphic created by Ursula Alonso).*

Effect of groundwater chemistry

In order for mass loss to occur at the interface of the extruding solid network, a system where inter-particle interactions are rather weak or repulsive must exist. Although interaction potentials in extruding clay systems are yet to be explicitly defined, there is clearly a strong effect of electrolyte concentration. One of the main findings from the work on chemical erosion in horizontal fractures was that, for purified montmorillonites, mass loss was observed only below a threshold cation charge composition of ~8.6 meq. In other words chemical erosion occurs only under highly dilute solution conditions. The results for a number of tests are compiled in Figure 6 showing average mass loss rates as a function of contact solution cation charge equivalents. It is clear that average mass loss rates are sensitive to electrolyte concentration even under highly dilute conditions and given that deionized water will not be representative of an actual, dilute groundwater, the maximal zero charge limit case can be considered overly conservative. It should also be noted that, below the erosion threshold solution composition, average mass loss rates for the as-received bentonites are an order of magnitude lower than for the purified montmorillonites.

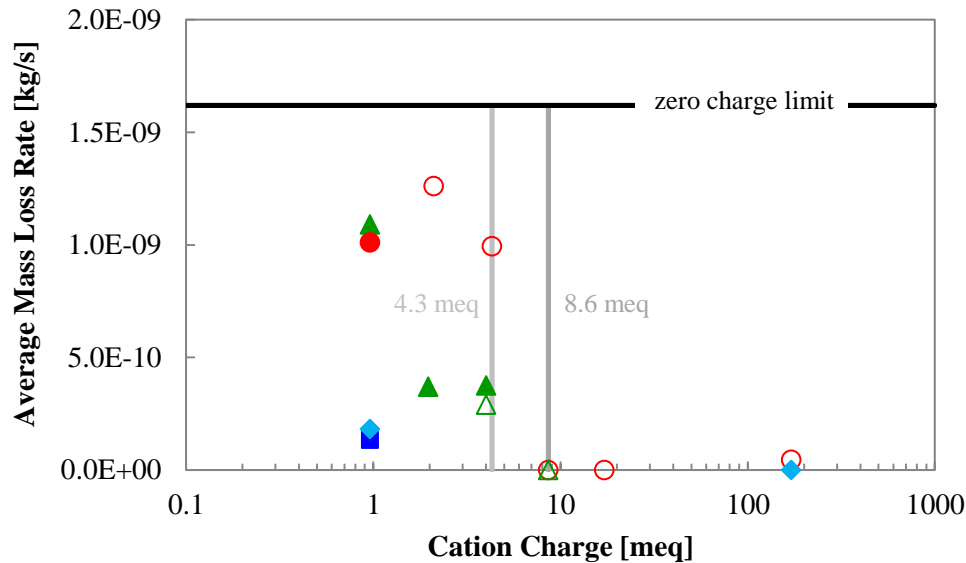


Figure 6. Average mass loss rates for various sample materials from horizontal, 1 mm aperture, artificial fracture tests as a function of cation charge equivalents for solutions flowing through the fracture systems. Filled red circles represent tests with sodium montmorillonite at a flow velocity of $\sim 10^{-6}$ m/s; open red circles represent tests with sodium montmorillonite at a flow velocity of $\sim 10^{-4}$ m/s; filled green triangles represent tests with 50/50 calcium/sodium montmorillonite at a flow velocity of $\sim 10^{-6}$ m/s; open green triangles represent tests with 50/50 calcium/sodium montmorillonite at a flow velocity of $\sim 10^{-4}$ m/s; filled blue squares represent tests with MX-80 bentonite at a flow velocity of $\sim 10^{-6}$ m/s; filled light blue diamonds represent tests with Milos bentonite at a flow velocity of $\sim 10^{-6}$ m/s. The zero charge limit line indicates the average mass loss rate observed for sodium montmorillonite against deionized water (zero cation charge) at a flow velocity of $\sim 10^{-4}$ m/s. All samples were emplaced at ~ 1.6 g/cm³.

Effect of flow velocity

Average mass loss rates for those tests where mass loss was observed, with flow expressed in terms of flow velocity, are plotted in Figure 7. The overall mass loss rates for the tests with the highest levels of observed erosion, i.e. the tests conducted with sodium montmorillonite against deionized water, appear to be well-correlated with flow velocity (proportionate to the power of 0.15). On the other hand, for those tests conducted under slightly less dilute conditions, clear attenuation in mass loss relative to the maximum, bounding erosion rates was observed. This attenuation can be attributed to solution composition effects independently, as well as in combination with material composition effects. As discussed previously, such effects indicate that the use of maximum erosion rates to estimate mass loss anywhere below a stability limit will lead to conservative predictions in the horizontal fracture case.

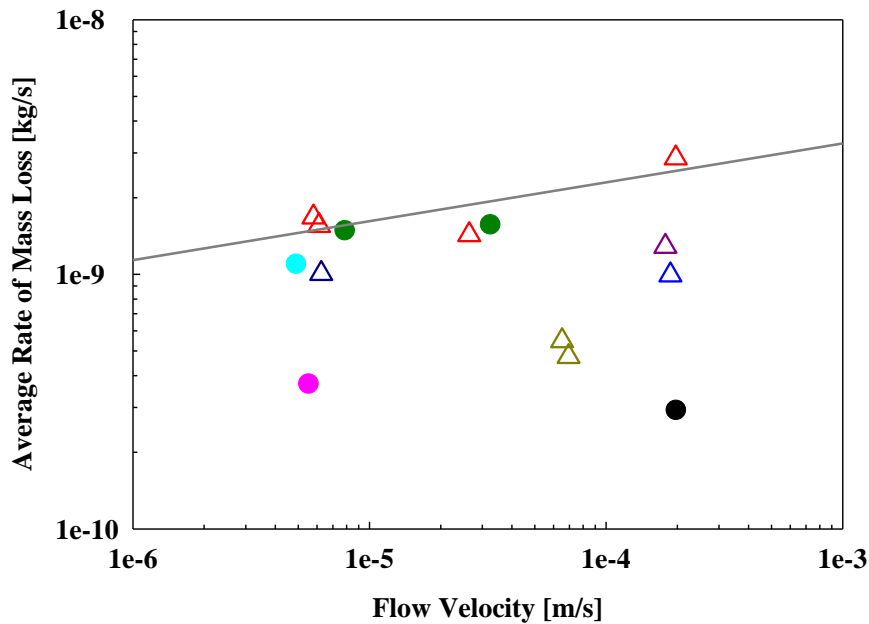


Figure 7. Experimentally observed mass loss rates from 1 mm aperture, horizontal artificial fracture tests expressed in terms of flow velocity. Open red triangles represent tests with sodium montmorillonite against deionized water; filled green circles represent tests with 50/50 calcium/sodium montmorillonite against deionized water; open dark blue triangle represents test with sodium montmorillonite against a 0.68 mM NaCl + 0.14 mM CaCl₂ solution; filled cyan circle represents test with 50/50 calcium/sodium montmorillonite against a 0.68 mM NaCl + 0.14 mM CaCl₂ solution; filled pink circle represents test with 50/50 calcium/sodium montmorillonite against a 1.36 mM NaCl + 0.28 mM CaCl₂ solution; open olive triangles represent tests with sodium montmorillonite against deionized water in a 0.1 mm aperture fracture; open purple triangle represents test with sodium montmorillonite against 2.1 mM NaCl; open blue triangle represents test with sodium montmorillonite against 4.3 mM NaCl; filled black circle represents test with 50/50 calcium/sodium montmorillonite against 4mM NaCl. Line corresponds to power law fit to mass loss data from tests with sodium montmorillonite against deionized water.

A possible explanation for this attenuated erosion may be due to structure formation and evolution of the eroding material. Evidence for this possibility is displayed in Figure 8 and was clearly evident only for the more calcium-rich systems (solution composition and/or material composition).

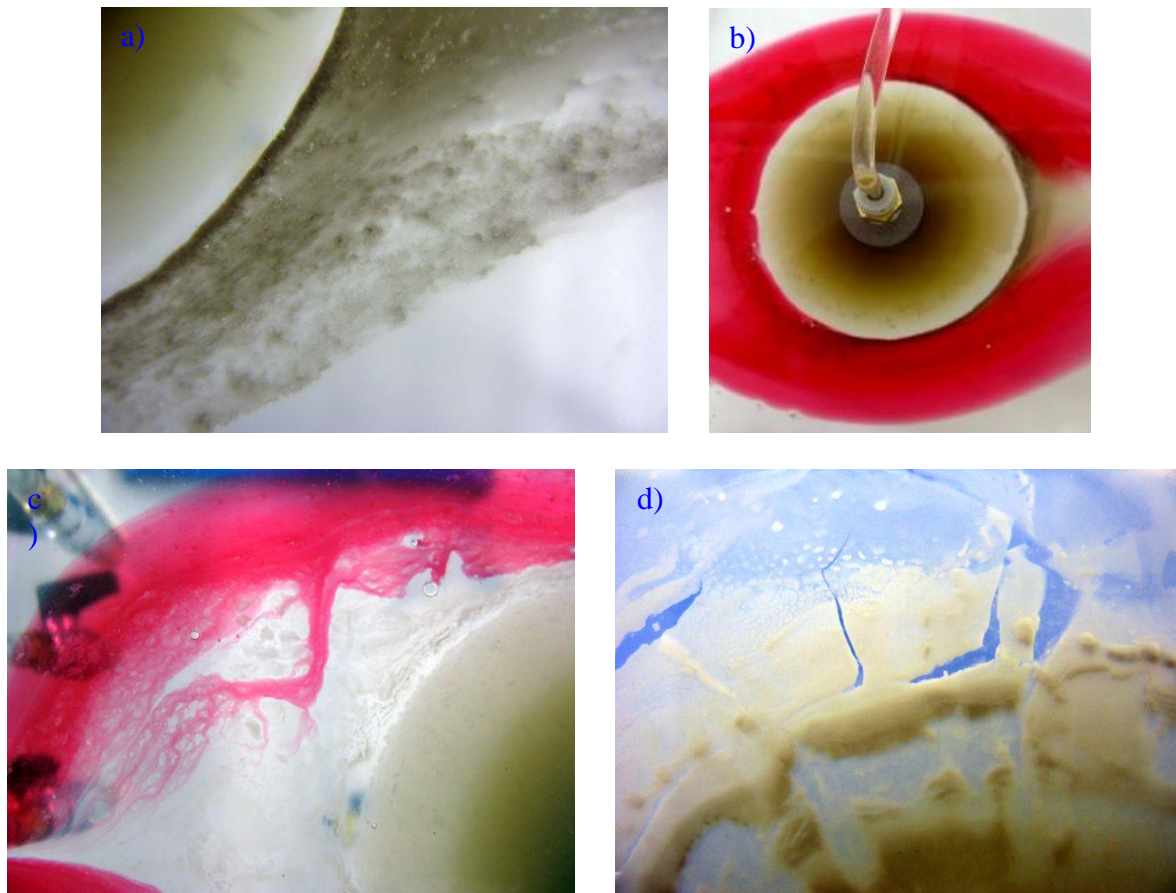


Figure 8. *Photographic images showing a) the interface between the inner zone of extruded material and the outer zone of eroding material for a test with sodium montmorillonite against deionized water at 456 h, b) flow visualization of the same test highlighting the permeability of the eroding material zone and the relative impermeability of the extruded material zone, c) flow visualization of a test with 50/50 calcium/sodium montmorillonite against 4 mM NaCl indicating the semi-permeability of the eroding material zone and d) the extrusion/erosion interface from a test with 50/50 calcium/sodium montmorillonite against double strength Grimsel groundwater simulant demonstrating that the eroding material forms into extended sheets of rigid, coherent material.*

Effect of fracture aperture

The effect of fracture aperture on mass loss can also be observed from Figure 7. Specifically, accounting for flow velocity, the average mass loss rates for sodium montmorillonite against deionized water in 0.1 mm aperture fractures are nearly one order of magnitude lower than for sodium montmorillonite against deionized water in 1 mm aperture fractures for samples emplaced at the same dimensions and densities. Overall, these results are consistent with a surface-area controlling effect on mass loss.

Effect of fracture slope angle

Figure 9 shows a set of photographic images from tests on sodium montmorillonite, 50/50 calcium/sodium montmorillonite and MX-80 bentonite in 1 mm aperture, horizontal (top images) and 45° sloped fractures (bottom images) against the same dilute solution flowing through the fractures at identical flowrates. For the purified montmorillonites, the tests in the horizontal fractures (Fig. 9a and 9b) show that mass is lost from the extruded source material through dispersive release and transport. A similar process occurs for MX-80 sample also (Fig. 9c), but the concentration of dispersed material is much lower and not distinguishable in the image. With regard to the sloped fracture tests on the other hand (Fig. 9d, 9e and 9f), mass appears to be lost from the extruded source material in a completely different fashion, i.e., via structural collapse and sedimentation. Furthermore steady state extrusion distances are observed in the horizontal fracture cases but not for the sloped fracture systems where some collapse of the original extruded zones themselves occur. As slope angle is the only experimental variable that differs between the tests pictured in Figure 9, it can only be slope angle that causes the observed differences.

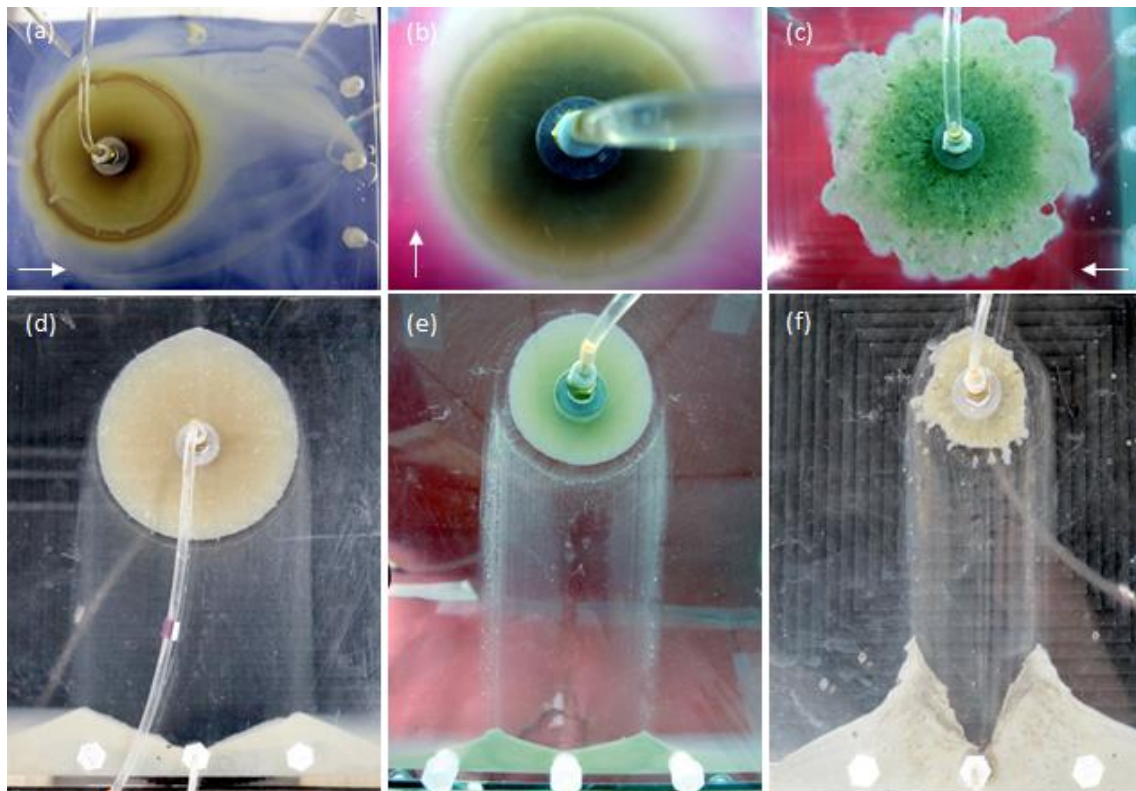


Figure 9. Photographic images of extrusion and mass loss of sodium montmorillonite in a (a) horizontal and (d) 45° sloped fracture, 50/50 calcium/sodium montmorillonite in a (b) horizontal and (e) 45° sloped fracture and MX-80 bentonite in a (c) horizontal and (f) 45° sloped fracture. All of the tests pictured were conducted in 1 mm aperture fractures with a dilute solution (0.68 mM NaCl + 0.14 mM CaCl₂) flowing through the fractures at ~0.09 ml/min. The direction of flow in the horizontal fractures is as indicated by the arrows; the direction of flow in the 45° sloped fractures is from the top of the images to the bottom.

Average mass loss rates among a series of artificial fracture tests with sodium montmorillonite, 50/50 calcium/sodium montmorillonite and MX-80 bentonite from 0° to 90° slope angles are compared in Figure 10. In every case conducting tests, that in all other respects are identical, at larger slope angles leads to increased mass loss rates. Specifically, in the tests with sodium montmorillonite and 50/50 calcium/sodium montmorillonite, rate increases of 96% and 50% and 17% and 5% were observed in the two systems for fracture slope angle increases from 0° to 45° and 45° to 90°, respectively. The modest increases of the average mass loss rates at slope angles from 45° and 90° indicates that whatever additional force is imposed on the extruding material at 90° does not lead to significantly more mass loss (structural collapse and sedimentation) than is already achieved at 45°. More dramatically, in tests with MX-80 bentonite, the relative rate increases were 340% and 130% for fracture slope angle increases from 0° to 25° and 25° to 45°, respectively. Overall, the relative rate increase was nearly one order of magnitude for the tests with MX-80 bentonite from 0° to 45° fracture slope angles.

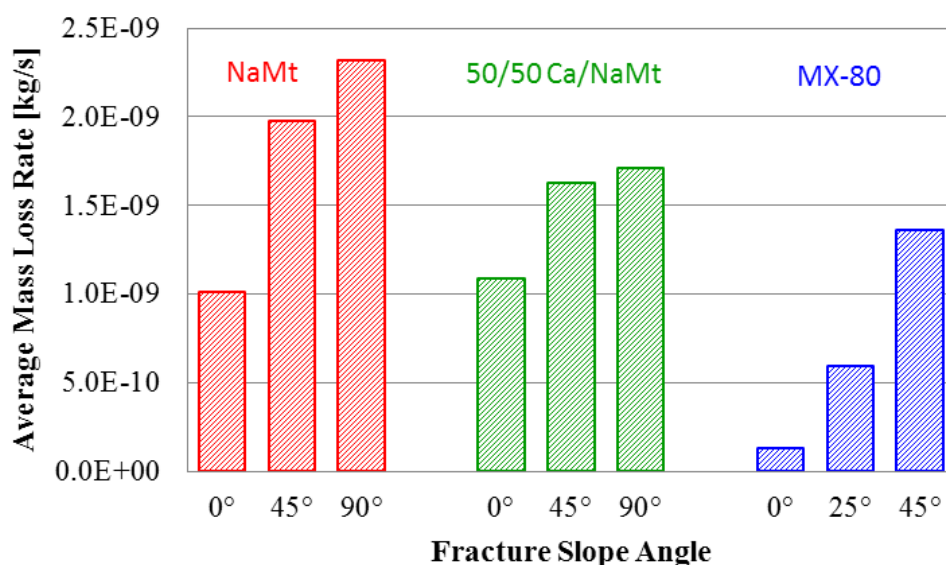


Figure 10. Average mass loss rates from artificial fracture tests with sodium montmorillonite (red) in horizontal (0° slope angle) and sloped (45° and 90° slope angles) fractures, 50/50 calcium/sodium montmorillonite (green) in horizontal (0° slope angle) and sloped (45° and 90° slope angles) fractures and MX-80 bentonite (blue) in horizontal (0° slope angle) and sloped (25° and 45° slope angles) fractures. All of the tests were conducted in 1 mm aperture fractures with a dilute solution (0.68 mM NaCl + 0.14 mM CaCl₂) flowing through the fractures at ~0.09 ml/min.

As for the horizontal fracture case above, the effect of solution composition on mass loss was examined in sloped fracture environments as well. Similarly, the stability of the (bentonite) buffer material to chemical erosion in sloped fractures has been analysed as a function of contact solution composition (in terms of cation charge equivalents) from ~170 meq (10 g/L NaCl) to zero (DI water). The results for a number of tests conducted at 45° slope angles are compiled in Figure 11 showing average mass loss rates as a function of contact solution cation charge equivalents. It appears that, irrespective of fracture slope angle, at cation charge concentrations ≥ 8.6 meq, the rate of erosion for all of the tested materials is effectively zero.

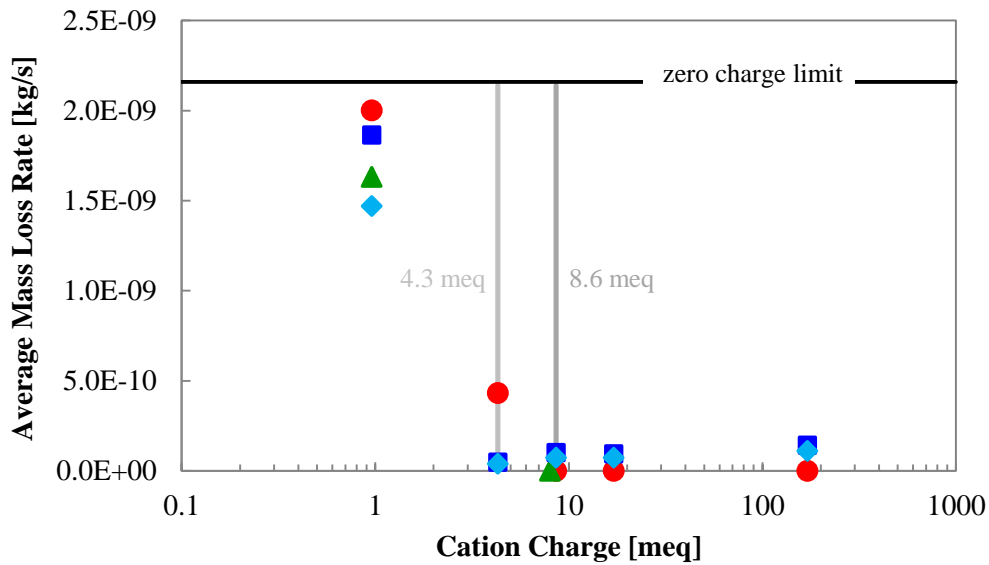


Figure 11. Average mass loss rates for various sample materials from 45° slope angle, 1 mm aperture, artificial fracture tests as a function of cation charge equivalents for solutions flowing at $\sim 10^{-6}$ m/s down the fracture systems. Filled red circles represent tests with sodium montmorillonite; filled green triangles represent tests with 50/50 calcium/sodium montmorillonite; filled blue squares represent tests with MX-80 bentonite; filled light blue diamonds represent tests with Milos bentonite. The zero charge limit line indicates the average mass loss rate observed for sodium montmorillonite against deionized water (zero cation charge) at a flow velocity of $\sim 10^{-6}$ m/s. All samples were emplaced at ~ 1.6 g/cm³.

Despite the mass loss mechanisms being different in the horizontal (dispersion and transport) and 45° fracture slope angle (structural collapse and sedimentation) cases, they are both operational only under similar chemical environments, i.e., cation charge concentrations < 8.6 meq. Observations of mass loss at or above 8.6 meq are not attributed to any continuous erosive condition, but rather to a slaking phenomenon (i.e., disintegration or breakdown of aggregates on wetting with release of trapped air) or loss on emplacement.

The effect of flow velocity on mass loss was also examined in sloped fracture environments. Average mass loss rates for tests with sodium montmorillonite are plotted in Figure 12 as a function of flow velocity. Increasing the flow down the fracture from zero (stagnant conditions) to 10^{-6} m/s results in a factor of three increase in mass loss; further increasing the flow velocity by roughly two orders of magnitude yields only a 15% additional increase in mass loss. By contrast, a similar, two order of magnitude flow velocity increase in horizontal fracture systems leads to a 50% increase in mass loss (see Figure 7). The different effects of flow velocity on mass loss between horizontal and sloped fractures are consistent with the concept of different mass loss mechanisms in these systems.

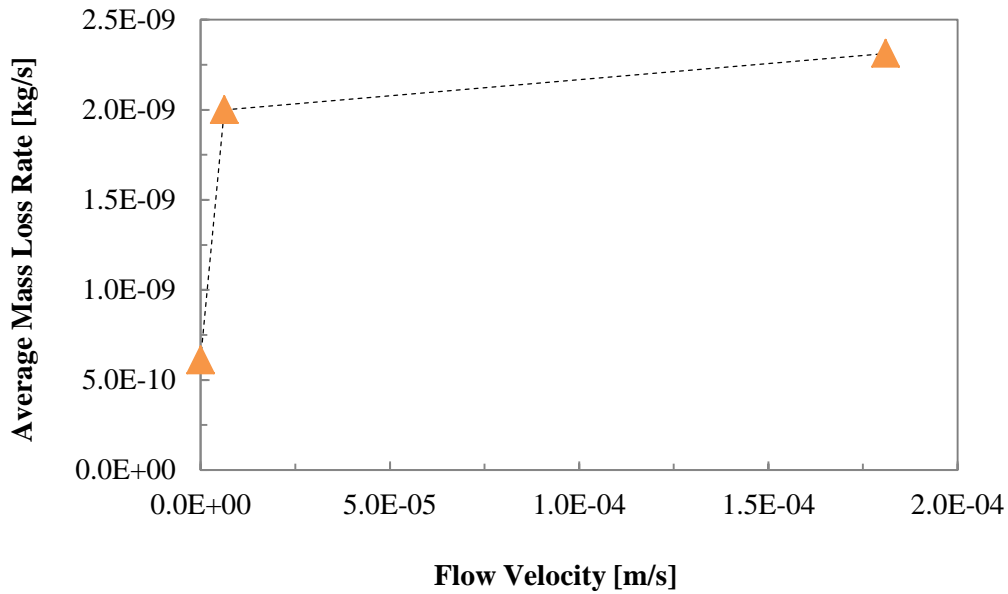


Figure 12. Average mass loss rates as a function of flow velocity for sodium montmorillonite against 0.68 mM NaCl + 0.14 mM CaCl₂ solutions in 45° slope angle, 1 mm aperture, artificial fracture tests.

Lastly, the effect of fracture aperture on mass loss was examined in sloped fractures. The average mass loss rate for as-received MX-80 bentonite against a 0.68 mM NaCl + 0.14 mM CaCl₂ solution in a 0.1 mm aperture fracture at a 45° slope angle is more than one order of magnitude lower than for the same in a 1 mm aperture fracture for samples emplaced at the same dimensions and densities. As with similar observations in horizontal fractures, these results are consistent with a surface-area controlling effect on mass loss.

Accessory Minerals

Artificial fracture tests have provided evidence that following erosive loss of montmorillonite through contact with dilute groundwater at a transmissive fracture interface, accessory phases (from montmorillonite mixed with various insoluble minerals and from as-received bentonite itself) remain behind and build-up at the extrusion interface (see Figure 13). However, it has not yet been demonstrated that such build-up leads to any attenuation of mass loss.

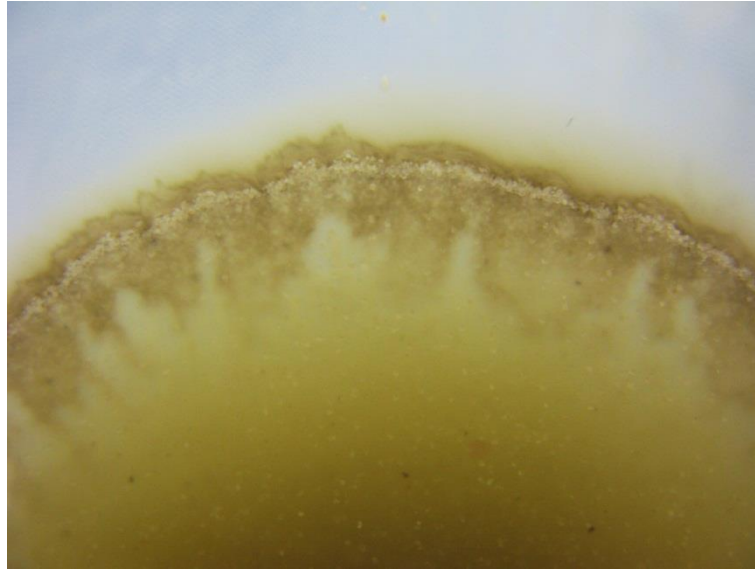


Figure 13. *Overhead photographic image of a 1 mm aperture, horizontal artificial fracture test with a sample comprised of sand and sodium montmorillonite; sand layer formation at the extrusion/erosion interface is clearly visible.*

Scaling

When considering the results of artificial fracture tests in the context of repository performance assessment, the main uncertainty concerns the question of scaling. This concern is most pertinent with regard to normalized erosion results as it is rather easy to upscale these results to repository dimensions assuming the rate of extrusions of material into the fractures are the same. However, this assumption has not been systematically examined (e.g., are the small-scale artificial fracture tests mass limited? Is the extrusion process affected by the presence of rough rock surfaces?) and if it does not hold may lead to inaccurate erosion estimates at repository scale.

An additional aspect of bentonite buffer material that requires comment is that it contains a significant amount of non-clay material accessory mineral phases.

MAIN CONCLUSION FROM RHEOLOGICAL STUDIES AT B+TECH

Rheological studies were conducted in order to study the mechanical properties of the expanding gel-like phase that develops when clay material swells into thin fractures. Learning about the mechanical strength of the expanding phase was a primary goal, and gaining information about the structure of the expanding phase was a secondary goal. Both goals were achieved, at least partially.

The experiments were performed under a variety of conditions simulating extruding clay material and detailed information regarding experimental protocols can be found in (Eriksson and Schatz 2015).

The main findings can be summarized as follows (Eriksson and Schatz 2015, Hedström,

Nilsson and Eriksson 2015):

➤ Shear viscosities were very low for montmorillonite suspensions at solids contents up to 1 vol %. Almost Newtonian flow behavior was observed for most samples. Pronounced shear thinning was observed only for montmorillonite suspensions at 17 mM NaCl, which implies the existence of volume spanning structures in the suspensions. All low solids content samples sediment, which was also observed to occur in artificial fracture tests in the area outside of the expanding gel-like phase. Considering this, no stable colloidal sol phases are expected to exist in fractures due to detached clay material since the detached particles will either sediment (due to flocculation) or be transported further away as single, isolated particles (consisting of a few clay platelets at the most). It is uncertain how far these particles would be able to travel, since their long-term stability is unknown.

➤ A transition from liquid-like or phase separating (sedimenting) behavior to solid-like behavior was observed to occur between 2 – 4 vol % montmorillonite solids content. Consequently, the solids content of montmorillonite at the outer rim of the expanding gel-like phase is likely within this range.

➤ Solid-like montmorillonite suspensions (i.e. solids contents ≥ 4 vol %) display viscoelastic character with relaxation times on the order of several hours. On shorter timescales the response to a small applied strain is mostly elastic, meaning that when the strain is removed the structure reverts back to its original form. On longer timescales (hours) the structure relaxes, which means that structural rearrangements occur. Based on these and other observations, the gel-like expanding phase does not behave like a solid elastic body, except at short timescales, which can be considered irrelevant compared to the repository lifetime. Furthermore, observations indicate that the expanding phase consists of zones of higher density (clay particle agglomerates) and lower density (water). When these systems are subject to an applied strain, the stress response mainly originates from frictional forces between the agglomerates, and during relaxation these agglomerates are slowly deformed and displaced in order to reduce the stress in the system.

➤ Apart from gravity, the only other process exerting strain on the expanding gel-like phase under normal circumstances is the water flowing around it. The shear forces experienced by the outer rim of the expanding gel-like phase were compared to experimentally determined yield stresses of montmorillonite suspensions comparable in composition to the expanding gel-like phase (Eriksson and Schatz 2015). It was found that the shear stress on the outer rim (at realistic groundwater flow velocities) is much lower than the yield stress of the gel-like expanding phase and therefore it was considered highly unlikely that mechanical shear can perturb the gel-like phase in any way, including detaching particles from the interface. This conclusion requires that the outer rim interface is not too rough, and that a low viscosity liquid (i.e. water) is exerting the shear stress. Based on OCT imaging (see Fig. 14) both requirements seem to be met, at least in artificial fracture tests.

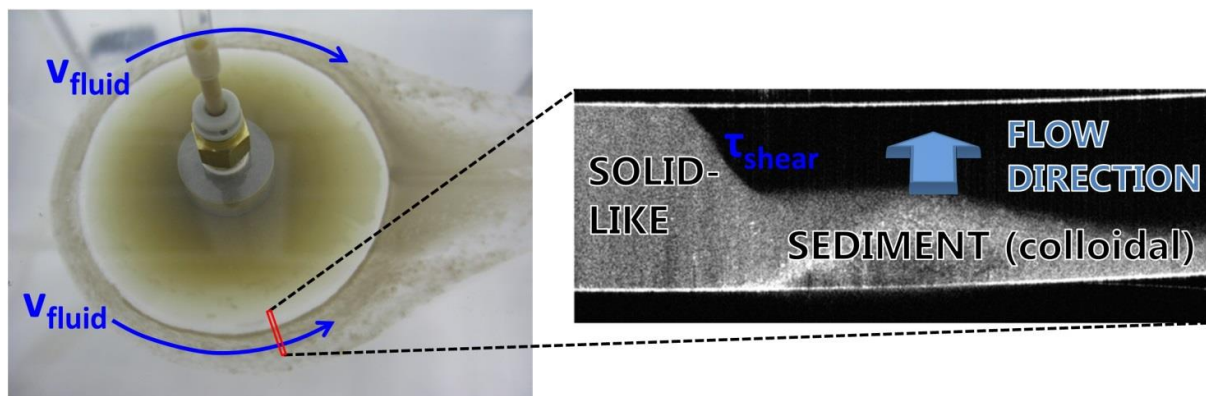


Figure 14. *On the left: Overhead photograph of an artificial fracture test. The expanding solid-like phase can be clearly identified as the white-rimmed circular zone slightly to the left of center in the picture. The colloidal (sedimenting) phase is also visible outside of the solid-like phase as a light brown-colored zone that apparently arranges itself along the water flow path. On the right: Optical Coherence Tomography (OCT) image of the region marked with red color in the photograph. The OCT image is a side-view of the interfacial zone from which the sharpness of the solid-liquid interface can be clearly seen.*

However, erosive mass loss does occur at some conditions, and the detachment mechanism, if not due to mechanical shear, must be due to some chemical process. In this case it is most likely the swelling process itself that leads to particle detachment. From a chemical, and somewhat simplified perspective, detachment may occur when the driving force for water uptake (of osmotic nature) overcomes the attractive forces between the clay platelets. In such a situation, the clay platelets are driven further and further apart until the attraction between them has become so weak that they can be picked up by the water flowing around the rim or they simply diffuse away (if there is no water flow). Hence, the particles that are detached and transported away are very small (single platelets or aggregates consisting of a few platelets), because larger particles would sediment. Of course, some of these particles will later downstream collide with other particles to form larger aggregates that sediment, while others escape further downstream, but as mentioned before, it is uncertain how far they could travel.

2) SUMMARY OF MAIN RESULTS FOR WP2 OBTAINED AT CLAY TECHNOLOGY AB

Materials and methods

The erosion studies reported here have been performed using Wyoming-type (Wy) montmorillonite extracted from MX-80 bentonite (American Colloid Co.). The montmorillonite was purified and ion-exchanged with NaCl or CaCl₂ to the homo-ionic form according to the procedure described in (Karnland *et al.* 2006). The purified montmorillonite is referred to as Wy-Me, where Me is the main exchangeable cation.

Most experiments in this study have been conducted using Wy-Na. There are two major reasons for working with Wy-Na: First, Na-montmorillonite show essentially unlimited swelling below the critical coagulation concentration (CCC), i.e. it turns into a sol, which is the reason for studying the erosion process under dilute conditions in the first place. Second, Wy-Na has the highest CCC (~20 mM NaCl) of all the clays investigated in Deliverable D4.7. Thus erosion rates obtained using Wy-Na are pessimistic estimates, compared to the conceivable future conditions in a high-level waste (HLW) repository.

Wy-Ca, on the other hand, is not sol-forming (Birgersson *et al.* 2009) so in this study, erosion experiments using Wy-Ca have not been performed. However, mixed Ca/Na-montmorillonite was found to form sol and erode in deionized (DI) water when the Na⁺ content was >20% of the cation exchange capacity (CEC) (Birgersson *et al.* 2009, Hedström *et al.* 2011) in line with earlier findings (Shainberg and Kaiserman 1969). A Wy-Ca/Na montmorillonite prepared from mixing equal amount of powdered Wy-Ca and Wy-Na montmorillonite is therefore included in the present study. In this montmorillonite 50% of CEC is compensated by Ca²⁺ and 50% by Na⁺. In the following this clay will be referred to either as Wy-Ca/Na or as Wy-50/50.

Equipment

The artificial fractures, made of poly(methyl methacrylate), were square with an inside dimensions 21 cm by 21 cm. In the set of experiments reported here, two apertures, 120 μm and 240 μm have been used. The artificial fracture is equipped with an inlet and outlet, allowing us to flow various solutions through the cell (Figure 15).

Both on the inlet and outlet side there is a trench or narrow slot. On the outlet side some of the eroded material may gather there so the outlet slot is equipped with an additional inlet and outlet. This allows for flushing the outlet slot ensuring that all eroded material can be gathered. At the center of the fracture system there is room for a clay disk of diameter 35 mm and thickness ~10 mm. The clay is contacted to water only via the slit.

The amount of eroded montmorillonite was evaluated from the turbidity of the effluent, using a portable turbidimeter (TN-100, Eutech Instruments). The light source in the turbidimeter is an infrared-emitting (850 nm) diode. The intensity of the scattered light is directly converted to nephelometric turbidity units (NTU) by the instrument. At low clay concentrations (<5 g/L), the turbidity response have been found to be linear. The mass of eroded clay particles can thus be calculated through the equation $m_{\text{clay}}=(N \cdot V)/114$ where m_{clay} is the mass of the eroded clay (g), N is the turbidity (NTU) and V is the volume of the suspension (L) (Birgersson *et al.* 2009).

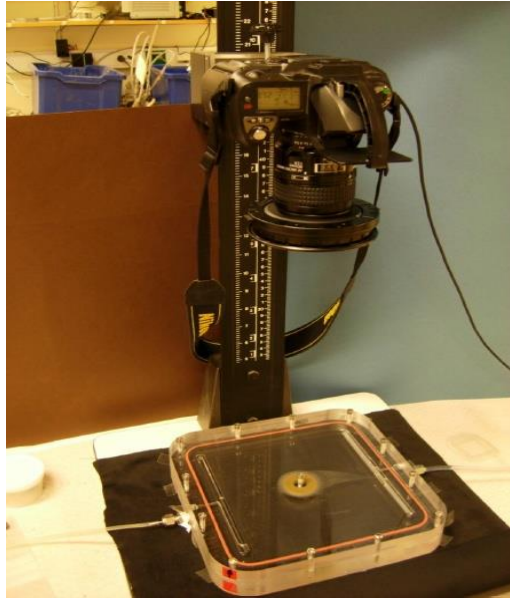


Figure 15. *Experimental set-up used for erosion experiment at ClayTech.*

Method

The montmorillonite was dried *in vacuo* overnight, followed by saturation with deionized water in a test cell similar to the ones used by ClayTech for measuring swelling pressures (Karnland *et al.* 2006). The initial dry density of the montmorillonite is 1257 kg/m^3 which gives a water-saturated density of 1800 kg/m^3 . The water-saturated clay disk was transferred to the artificial fracture, with care taken not to allow the clay to dry. The fracture was closed and filled with degassed deionized (DI) water.

During free swelling experiments, the artificial fracture was filled with degassed DI water, after which the clay was allowed to swell into the fracture. This was photographically documented, with pictures taken at suitable intervals depending on the rate of expansion.

During erosion measurement experiments, aqueous solution, also prepared from degassed DI water, was flowed through the artificial fracture. The start- and end times of the erosion measurement were recorded. When the flow was stopped, the collected suspension was weighted. The outlet slot was flushed with degassed DI water to collect eroded material which had gathered in the outlet slot, and the flushed-through suspension was also weighted. Turbidity measurements were used to determine the amount of eroded colloidal clay particles in both water volumes.

Results and discussion

Free swelling – deionized water

The free swelling behavior was investigated at two different fracture apertures, $120 \mu\text{m}$ and $240 \mu\text{m}$, in DI water. Initially, the swelling into the fracture progressed rapidly at both $120 \mu\text{m}$ and $240 \mu\text{m}$. While the swelling progressively slows down, during the experimental time scale it does not cease completely. At $120 \mu\text{m}$, closest to the clay disk we find a

repulsive paste, quite well-defined and thick enough to appear very bright in color (scattered light from the camera flashes) (Figure 16a). This paste is strong enough that as it expands, it pushes air bubbles in the fracture ahead of itself, rather than surrounding them. Further out, there is a sol of varying (and not yet determined) clay concentration. At the interface between the sol and the DI water a fingering instability occurs, akin to the Rayleigh-Taylor instability (RTI) that occurs when a denser liquid is placed on top of a less dense liquid and is pulled down by gravity. The RTI fingers are particularly well resolved in the thinner fracture Figure 16a. In this case it is not gravity that is the driving force for the RTI but water transport into the clay.

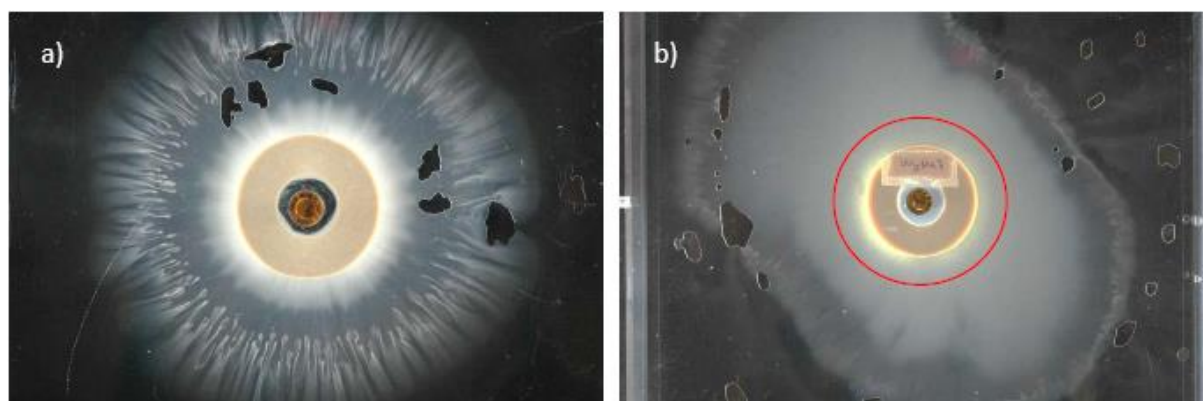


Figure 16: Free swelling in deionized water after 30 days at a) 120 μm aperture and b) 240 μm aperture. The red circle in b) shows the extent of extrusion (swelling) of paste (the brighter area outside the montmorillonite disk in a) into the fracture at 120 μm for comparison. When there is a rather high flow through the cell, all clay outside the brighter paste, is transported away.

The same phases, the thick paste and the sol, are found during free swelling at an aperture of 240 μm (Figure 16b). Also RTI can be found, although the fingers are less well-resolved at the broader aperture. As in the case of 120 μm aperture, the paste is sufficiently thick to push air bubbles ahead during swelling rather than encompassing them. For comparison, the edge of the corresponding paste is outlined in Figure 16b, which gives an idea of the difference in swelling capability at different apertures.

The paste, i.e., the thicker clay phase closest to the disk, is found to withstand the shear forces and not erode under our conditions, even at the highest flow rates. However, as swelling is a continuous process, particles that disperse from the paste to form a sol are easily flowed away into the fracture.

Free swelling – 25 mM NaCl-solution

The free swelling behavior in a solution with higher salinity was also investigated. When setting up this experiment, clay was mechanically extruded into the fracture when the fracture was closed, thus the clay in the fracture has the same density as in the disk. This point constitutes the starting point for swelling, and has been outlined with a red circle in Figure 17. During the initial 48 h, some swelling (1-2 mm) is evident.

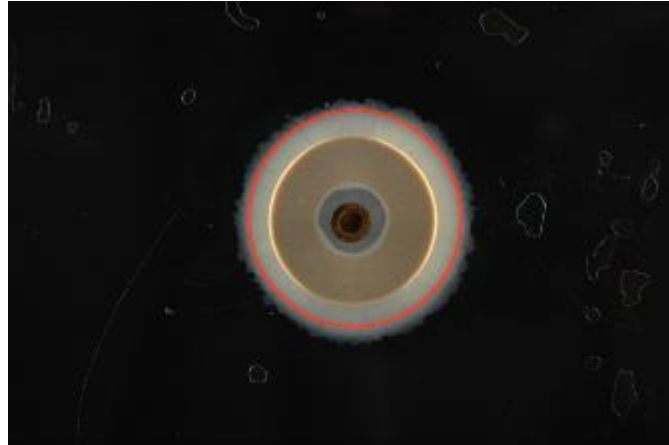


Figure 17 Free swelling in 25 mM NaCl-solution at an aperture of 120 μm . The saturated density of the montmorillonite is 1800 kg/m^3

Despite this, after the initial two days no more swelling is experienced and the clay appears to have formed a stable gel at the edges, which does not release clay particles into the fracture. Even with a flow of 25 mM NaCl-solution, there are no signs of erosion. In fact, decreasing the salinity to 20, 15 or 10 mM NaCl still causes no erosion during flow. In order to see any sign of erosion, the salinity of the solution had to be decreased to 5 mM NaCl. This suggests the presence of some sort of hysteresis, which might affect the montmorillonite loss in the actual HLW repository.

Erosion measurement Wy-Na

Initial erosion measurements were performed at a fracture aperture of 120 μm (Figure 18). The measurements commenced at 5 mM NaCl (aq). As expected, since CCC is in the vicinity of 20 mM, the erosion was found to increase with increasing flow rate. By raising the salinity to 10 mM NaCl (aq), erosion decreased. However, it was still increasing with flow rate. After increasing the salinity to 15 mM NaCl (aq), the erosion during the first 48 h was roughly half the erosion at the corresponding flow rates at 10 mM NaCl.

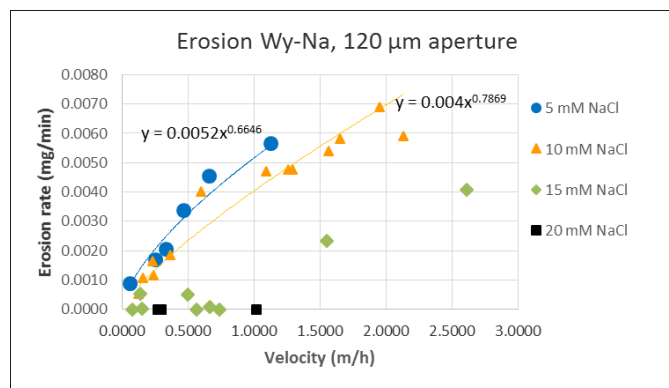


Figure 18. Erosion of Wy-Na in an artificial fracture with aperture 120 μm . Salinity of the flowing solution was increased from 5 mM NaCl to 20 mM NaCl.

Within a week, erosion had completely ceased or was below the detection limit. The salinity was further increased to 20 mM NaCl, as 20 mM NaCl has been reported as the CCC value of Wyoming montmorillonite clay (Birgersson *et al.* 2009). As expected, there were no signs of erosion. The erosion rate vs flow velocity is reasonably well captured with a power law for the lowest two NaCl concentrations with R^2 equal to 0.94 and 0.94 in the case of 5 mM and 10 mM, respectively.

After the salinity had been increased from 5 mM NaCl to 20 mM NaCl, we decided to test if erosion would commence at 10 mM NaCl as previously erosion ceased upon increasing the salinity from 10 mM NaCl to 15 mM NaCl. The salinity of the aqueous solution was first decreased to 15 mM NaCl before erosion measurements at 10 mM NaCl was started. Despite the fact that the erosion measurements were performed during a month's time, which is ample time for the clay to reach a new Donnan equilibrium with the new solution (Birgersson and Karnland 2009; Karnland and Hedström, 2012; Hsiao and Hedström, 2015), there were no signs of erosion during any of the measurements. Therefore, the salinity was decreased to 5 mM NaCl. Yet again, there were no signs of erosion during the initial measurements. However, after 16 days, erosion commenced. The erosion measurements were continued during two months, in order to investigate whether erosion during this time period reaches the erosion at the initial 5 mM NaCl-measurements. Despite this, the erosion did not appear to approach the earlier erosion levels (Figure 19). It is of course possible that given enough time, the erosion will be similar whether the NaCl-concentration is increased from deionized water, or decreased from a higher NaCl-concentration, but it is not obvious on this time scale. Consequently, there appear to be a considerable hysteresis effect, where the history of the clay sample appears to play a significant role in the erosion of montmorillonite clay. This illuminates the difficulty in reaching conclusions as to the CCC, the phase behavior or the erosion susceptibility of montmorillonite.

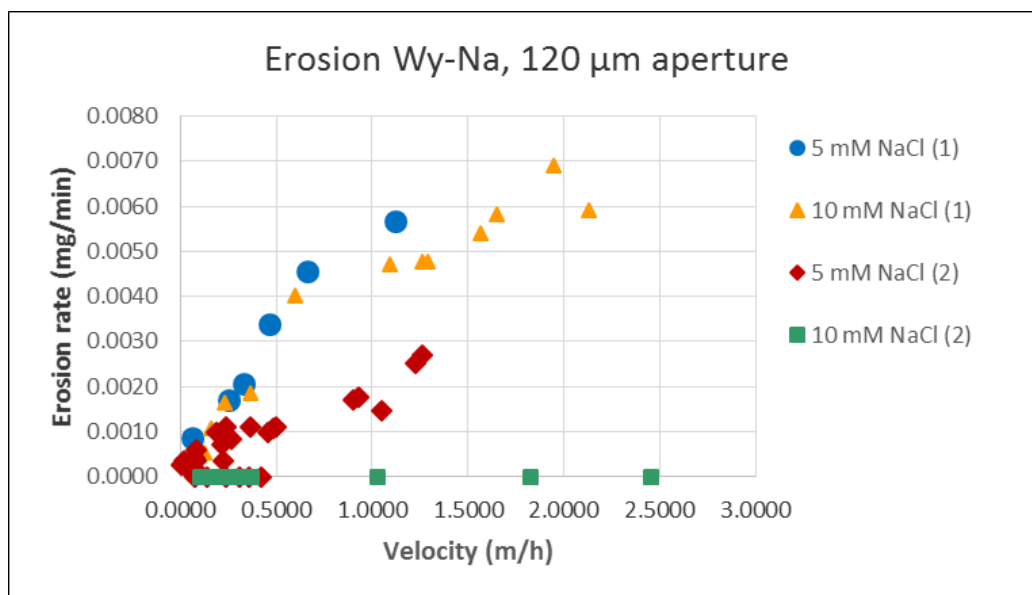


Figure 19. Erosion rates v.s flow velocity for the case where first the NaCl concentration in the flowing solution was increasing (1). After reaching 20 mM NaCl the concentration in the flowing solution was decreased (2).

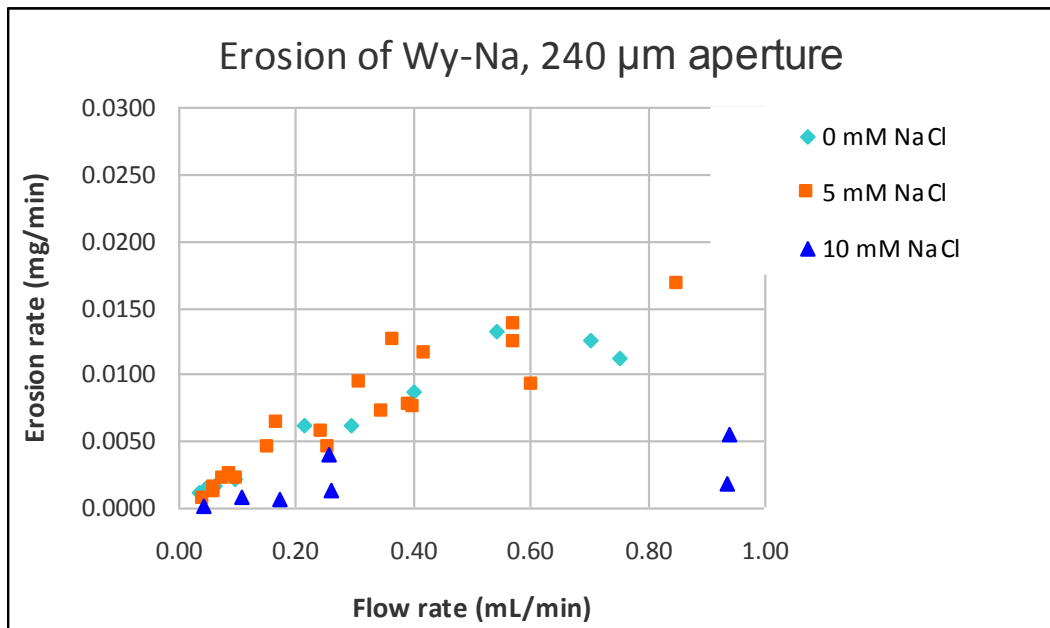


Figure 20. Erosion of Wy-Na in an artificial fracture with aperture 240 μm . Salinity was increased from 0 mM NaCl to 10 mM NaCl.

Erosion measurements at an aperture of 240 μm commenced with deionized water. When shifting to 5 mM NaCl-solution, the erosion difference at low flows was marginal, although the difference in erosion at higher flows was more significant (Figure 20).

Comparison of erosion at different fracture apertures

When we compare the erosion at different fracture apertures, we find that the erosion depends on the fracture aperture as well as salinity. One has to take into account that in Figure 18 the erosion rate is plotted against flow rate given as volume per time, thus at the same flow rate the flow velocity at the larger aperture is lower. Without any clay present the velocity would be precisely a factor two lower in the 240 μm fracture compared to the 120 μm fracture at the same flow rate. Due to larger extrusion of clay in the wider fracture the ratio in flow rate must be less than a factor two. The results in Figure 21 show that at 5 mM, erosion rate is larger in the wider fracture also taking velocity into account. However at 10 mM NaCl the erosion rates vs. flow velocity are more or less the same for the two apertures.

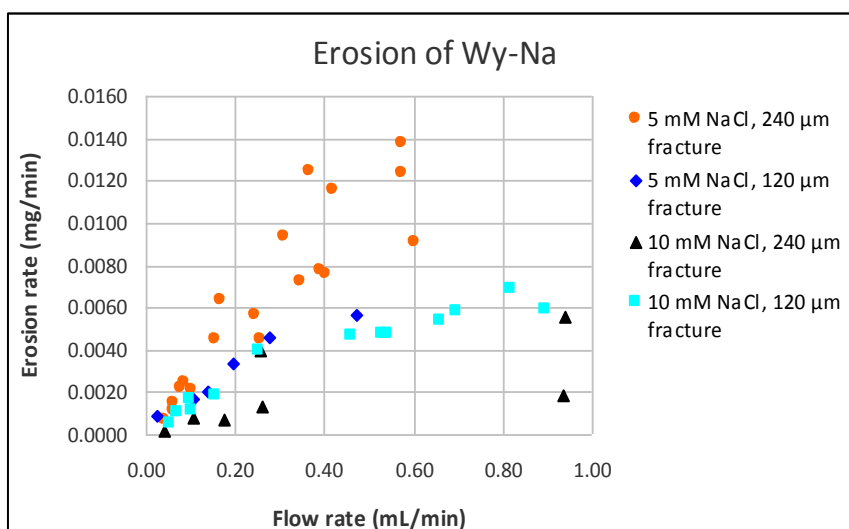


Figure 21. Comparison of erosion rates of Wy-Na in artificial fractures with apertures 120 μm and 240 μm . Salinity was increased from 0 mM NaCl to 10 mM NaCl.

Erosion from Wy-Ca/Na (Wy-50/50)-horizontal fracture

The mixed Wy-Ca/Na was water saturated in a test cell over a period of 9 days after which the montmorillonite disk was transferred to the artificial fracture setup (aperture 120 μm). The montmorillonite was contacted to DI and degassed water and was left to swell for 36 days under stagnant water conditions. The general free swelling behavior of Wy-50/50 is similar to Wy-Na (Figure 22), with the development of RTI fingers at interface to the water. After the free-swelling period DI water was flushed through the fracture to remove the sol. Then measurements of erosion under flowing conditions started using saline water with ionic strength from 1 mM to 20 mM. The ionic strength was set by NaCl but in order to avoid ion-exchange a small amount of CaCl₂ was added (1 μM to 10 μM depending on the NaCl concentration).

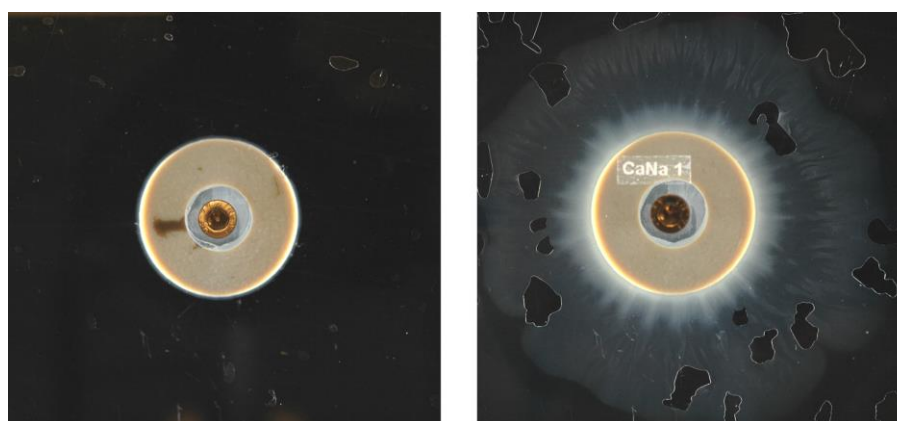


Figure 22. Free swelling of Wy-50/50 in deionized water and aperture of 120 μm . Left: Initial state. Right: The state after 36 days. The gas bubbles visible in the right picture presumably originate from gas that was trapped around (above and under) the montmorillonite disk at installation.

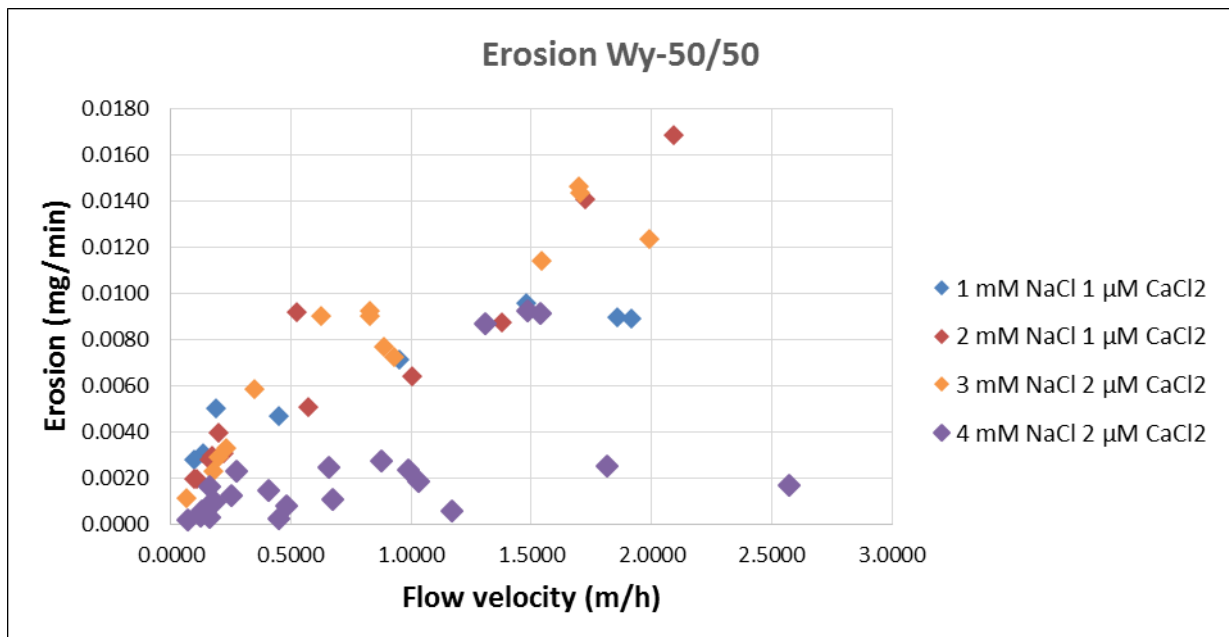


Figure 23. Erosion of Wy-Ca/Na in an artificial fracture with aperture 120 μm. Salinity was increased from 1 mM NaCl to 4 mM NaCl. A small μM CaCl₂ concentration is included to prevent ion exchange during the tests.

The results for ionic strength up to 4 mM are presented in Figure 23. For ionic strengths up to 3 mM the erosion rates behave similarly with erosion increasing with flow velocity. At 4 mM the erosion is generally lower at all flow velocities. Furthermore, there is no trend between flow velocity and erosion rate. There are three outliers in the 4 mM results (flow velocity ~1.5 m/h and erosion rates ~0.009 mg/min). Those measurements were made in the beginning, after switching from 3 mM to 4 mM solution and most likely reflects the behavior of Wy-Ca/Na at 3 mM and are not representative for the equilibrium conditions at 4 mM. In general, the erosion rates at 4 mM scatter around 0.001 mg/min which are close to the lowest measured rates for Wy-Na at 5 and 10 mM NaCl, but in contrast to the results for Wy-Na the dependence on flow velocity is absent.

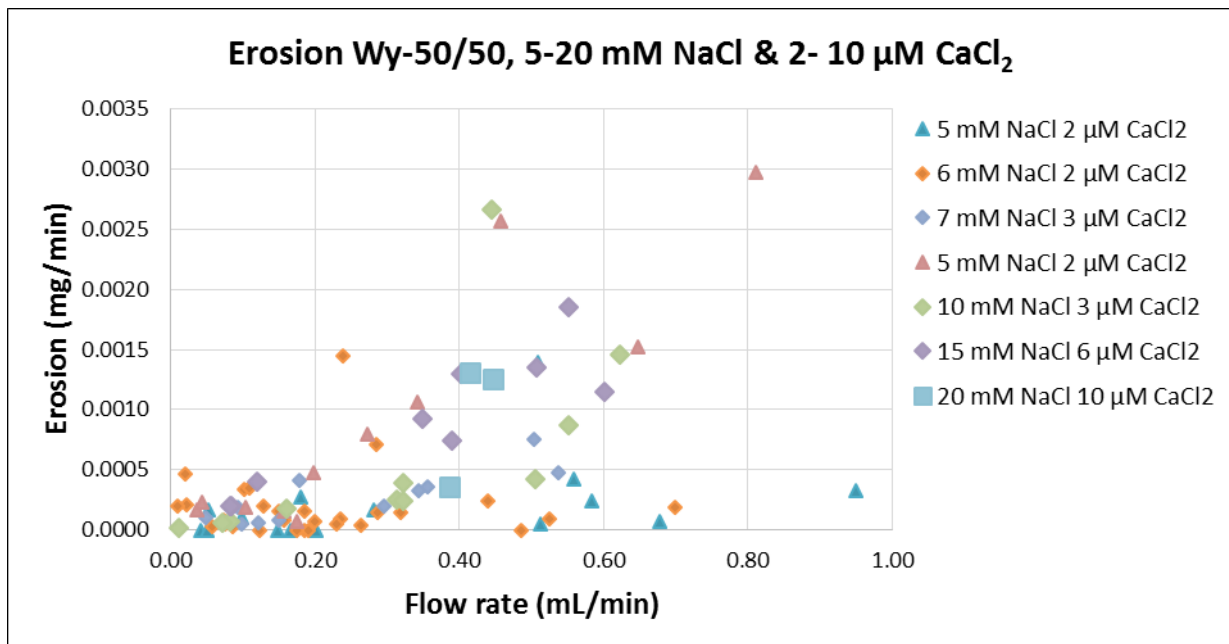


Figure 24. Erosion of Wy-Ca/Na in an artificial fracture with aperture 120 μm . Salinity was changed according to the order in the legend. The lowest salinity was 5 mM and the highest 20 mM. A small μM CaCl_2 concentration is included to prevent ion exchange during the tests.

The erosion did not stop at 4 mM so further tests at higher ionic strengths were conducted. Most measured erosion rates at ionic strengths between 5 and 20 mM were about a factor of two lower than the rates at 4 mM, but not showing any clear trend with increasing ionic strength (Figure 24). Possibly, there is a tendency that erosion increases for ionic strengths beyond 7 mM. After the erosion measurements at 7 mM were completed the ionic strength was lowered to 5 mM. The erosion rates measured at 5 mM after this change were higher than the erosion rates measured after ionic strength was increased from 4 to 5 mM. After the second period of erosion measurements at 5 mM the ionic strength was increased to 10, 15 and finally 20 mM. Interestingly, erosion did not stop even at 20 mM NaCl and 10 μM CaCl_2 .

At the lowest flow rates <0.2 mL/min all the erosion measurements in Figure 24 gave erosion rates below 0.0005 mg/min. With a diameter of the clay paste (initial disk + extruded zone) of 6 cm the above erosion rates correspond to a unit erosion rate of $3.7 \cdot 10^{-7}$ kg/m²·s. Under the assumption of a fracture aperture in the repository of 1 mm and a diameter of the clay paste of 2 m, the above unit erosion rate corresponds to an erosive mass loss < 0.08 kg/yr.

Returning to the erosion rates at NaCl concentrations from 1 to 4 mM, further insights can be gained by re-evaluating the data underlying the plot in Figure 23. In Figure 25 the variation of clay concentration in the effluent with flow velocity is shown. The clay concentration decreases with increasing velocity. This suggests that the paste-to-sol transition rate limits the erosion rate. At the higher flow velocities the concentration drops as the transfer of clay from paste to sol cannot keep up with the increased flow.

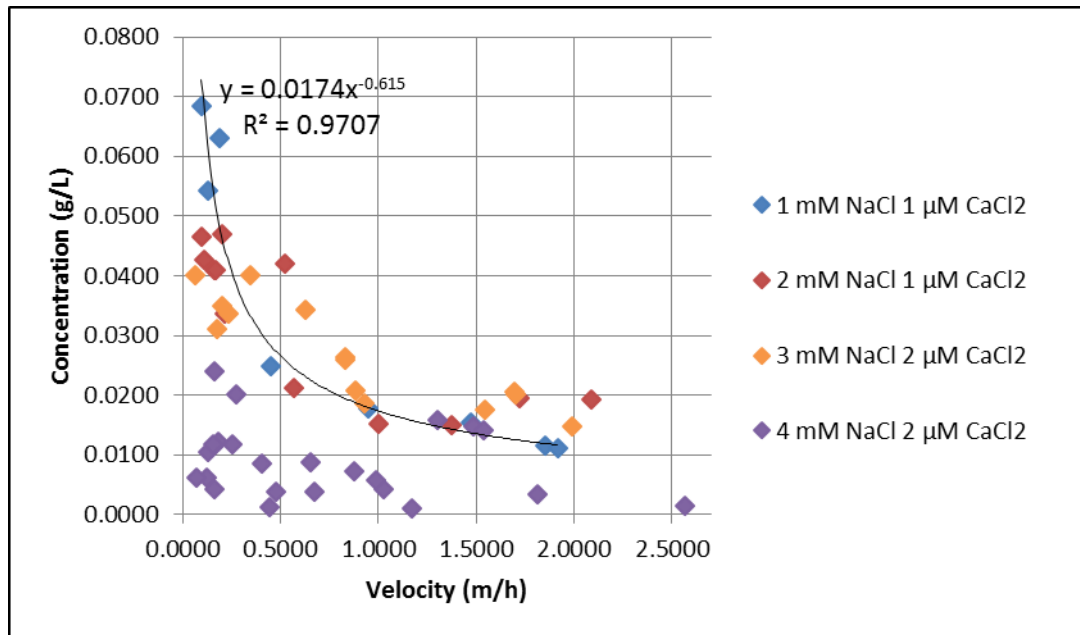


Figure 25. Clay concentration in effluent as a function of flow velocity.

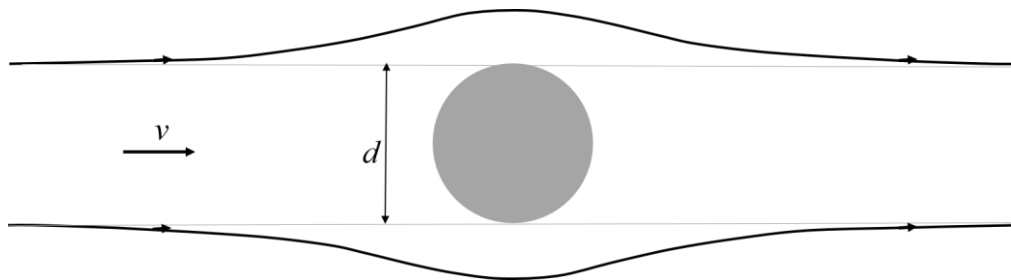


Figure 26. Flowlines around a circular clay region. Presumably flowlines originating outside the diameter, d , do not interact with the clay. The aperture of the fracture is a .

One may estimate the amount of eroded material per unit time, R_{ero} , as:

$$R_{\text{ero}} = vdaC_{\text{clay}}, \quad (1)$$

where v is the flow velocity, d is the diameter of the clay region, a the fracture aperture and C_{clay} the clay concentration in the volume that is limited by d (Figure 26). It is reasonable to assume that flowlines originating outside d do not interact with the clay, hence do not carry clay particles. Then that portion of the flow just dilute the clay concentration that is measured in the effluent. Thus C_{clay} is larger than the measured values (e.g., Figure 22) and can be obtained by multiplying the measured concentration by the lateral dimension (perpendicular to the flow) of the artificial fracture divided by d . In the case of 1 mM NaCl and the lowest velocity ($0.097\text{m/h}=850\text{m/year}$) in Figure 22, the diameter of the clay region, including the extruded portion, is 60 mm whereas the test cell width is 210 mm. C_{clay} is thus obtained

multiplying the concentrations in Figure 22 by $21/6=3.5$. At the lowest velocity the calculated C_{clay} is 0.24g/l. The unit erosion rate is evaluated to 65 kg/(m²·year). As seen in Figure 22 the clay concentration variation with flow velocity is well described with a power law. In the following we will argue that the calculated unit erosion rate is a pessimistic estimate as it is evaluated at a velocity that is at least an order of magnitude larger than realistic flow velocities in a repository during/after a glaciation.

When the flow velocity is reduced the clay concentration in the effluent is not increased by the same amount. For example assume the velocity is reduced by a factor of 100 the increase in clay concentration is just a factor of 16. R_{ero} in Eq. (1) could in this case only remain unchanged provided that the diameter d is increased about six times. In the present set-up, the swelling into the fracture is about 1 cm and it is reasonable to assume that when the system is scaled-up to repository dimensions the swelling into the fracture is similar as in the small scale test, i.e., on the order of centimetres. At a flow velocity of 850 m/year the anticipated diameter of the clay paste surrounding the canisters is around 2 m. For the erosion rate to be unchanged the diameter must increase to 12 m. The tests presented here never show any expansion of the denser region (that appear bright in the photographs in Figure 16 and Figure 22) beyond 10-15 mm into the 120 μm fracture. In the case of stagnant Grimsel water simulant and horizontal fracture the clay loss due to expansion into the fracture was the same after 12 days as after 6 days suggesting that the swelling process slows down significantly (see below). An additional factor not taken into account in the discussion above is the viscosity increase of the sol with increasing concentration. This would further reduce erosion.

Wy-Ca/Na in contact with Grimsel water simulant in horizontal and sloped fractures

We let Grimsel water (0.7 mM NaCl and 0.14 mM CaCl₂ in this study) represent glacial/post glacial conditions. Figure 27 shows the results from erosion tests using Grimsel water together with the results from 1 mM NaCl. The erosion rates using Grimsel water and a horizontal fracture are comparable to the previous findings for 1 mM NaCl. The results at zero flow velocity were obtained in stagnant water over a period of several days. The eroded amount represent the sol surrounding the paste, and this material was collected by flushing the fracture for 15-30 minutes using high flow. The erosion rate at zero velocity was calculated by dividing the eroded mass with the time of free “expansion” (rather paste-to-sol transition). The total amount was ~8 mg both after 6 days of swelling and after 12 days. This suggests that the paste-to sol transition only progresses as long as the sol is removed. In stagnant water the sol is only diluted which is a diffusive process and therefore slow.

For a sloped fracture, the sol is constantly removed due to gravity. Note that the sol is a liquid phase of higher density than water and gravity acts on this liquid. This gives in the case of a 45 degree slope angle an erosion rate of an order of magnitude higher than the one measured after 12 days under stagnant conditions in a horizontal fracture. Specifically the unit erosion rate becomes 170 kg/(m²·year). Using the example above of a clay paste with diameter of 2 m and a fracture aperture of 1 mm, the erosion from a sloped fracture (slope angle 45 degrees) amounts to approximately 1 kg/yr under glacial water conditions. Perhaps an aperture of 50 μm would be a more realistic case for a repository. Then the buffer clay loss would be 20 times less, which over a 10000 year period of glacial meltwater conditions would amount to 500 kg.

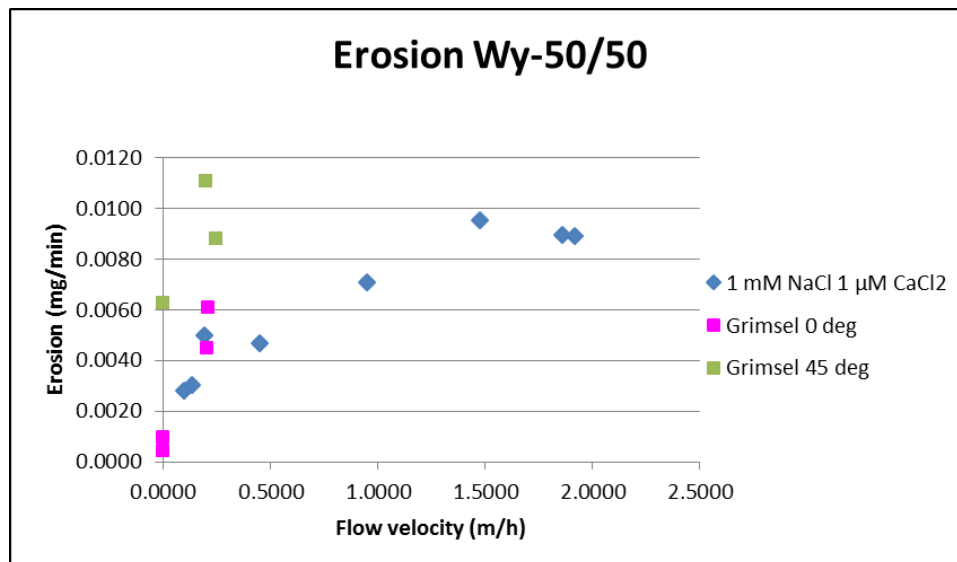


Figure 27. Erosion of Wy-Ca/Na in an artificial fracture with aperture 120 μm . Grimsel water has ionic strength of 1.12 mM which is comparable to 1 mM NaCl.

Conclusions

For Wy-Na we have confirmed the connection between the flow rate and the erosion, when the NaCl concentration is well below the CCC. As the salinity increases, erosion decreases. At an aperture of 120 μm , the erosion eventually ceases when the salinity in the system is 15 mM NaCl. For the aperture of 240 μm the test has not yet been performed above 10 mM but the tests at 10 mM NaCl indicate a clear reduction in erosion rate. In fact the erosion rates vs. flow velocity are the same for 120 and 240 μm apertures at 10 mM NaCl, possibly indicating the formation of stable structures at that salinity. However, more data are needed to verify this and to rule out other explanations.

Furthermore for Wy-Na, we see a hysteresis effect present, that is, the history of the clay will affect the erosion capability of the clay. That means that a montmorillonite clay that erodes at a salinity of 10 mM NaCl, might be completely stable against erosion, if it has previously had a higher salinity present, during which the clay particles at the clay-solution interface could form a gel. This suggests that not only is control of the boundary conditions of importance for evaluating erosion rates; awareness of the system's history seems also crucial. Erosion in sloped fractures showed an order of magnitude larger erosion rates compared to those obtained using horizontal fractures. As long as the sol is removed from the paste-sol interface, erosion was found to progress under glacial water conditions. The erosion rate obtained using Wy-50/50 montmorillonite was found to be approximately 170 $\text{kg}/(\text{m}^2 \cdot \text{year})$ in the case of stagnant conditions but 45 degree slope angle. Under horizontal conditions and a flow of 850 m/year the unit erosion rate was found to be 65 $\text{kg}/(\text{m}^2 \cdot \text{year})$.

3) SUMMARY OF MAIN RESULTS FOR WP2 OBTAINED AT CIEMAT

CIEMAT, performed erosion studies using different experimental sets-up. Experiments were designed with confined and compacted bentonite, simulating repository conditions. In a repository scenario, the water coming from the geological formation hydrates the bentonite and promotes its swelling. Due to its expansion, bentonite suffers a density loss, strongest at the gel front and, under favorable conditions; the gel can be transformed to sol. Bentonite particles release can be chemically induced (*static conditions*) or mechanically produced, when water flows along the bentonite surface (*dynamic conditions, with or without fracture*). Erosion experiments were mainly carried out with natural raw FEBEX bentonite, a Na-Ca-Mg bentonite with 92% smectite content and approximately 25 % of exchangeable Na (Huertas et al, 2000).

The cells used in the experiments can be seen in Figure 28 and Figure 29. To determine the generation of colloids under static (no flow) conditions a tablet of approximately 4 grams of compacted bentonite (1.2 to 1.65 g/cm³), was introduced in a stainless steel cylinder (Figure 28a) and located between two sintered stainless steel porous filters. The cell was closed by two open Delrin grids and immersed in the desired aqueous solution within a closed vessel (Figure 28b). The porous filters (Figure 28c) have a thickness of 3.1 mm, a mean pore size of 100 μ m and a porosity of approximately 40 %.

The filters allow the water to hydrate the bentonite and, at the same time, provide an open space for the extrusion of the gel formed, as well as for colloid formation and transport towards the aqueous phase.

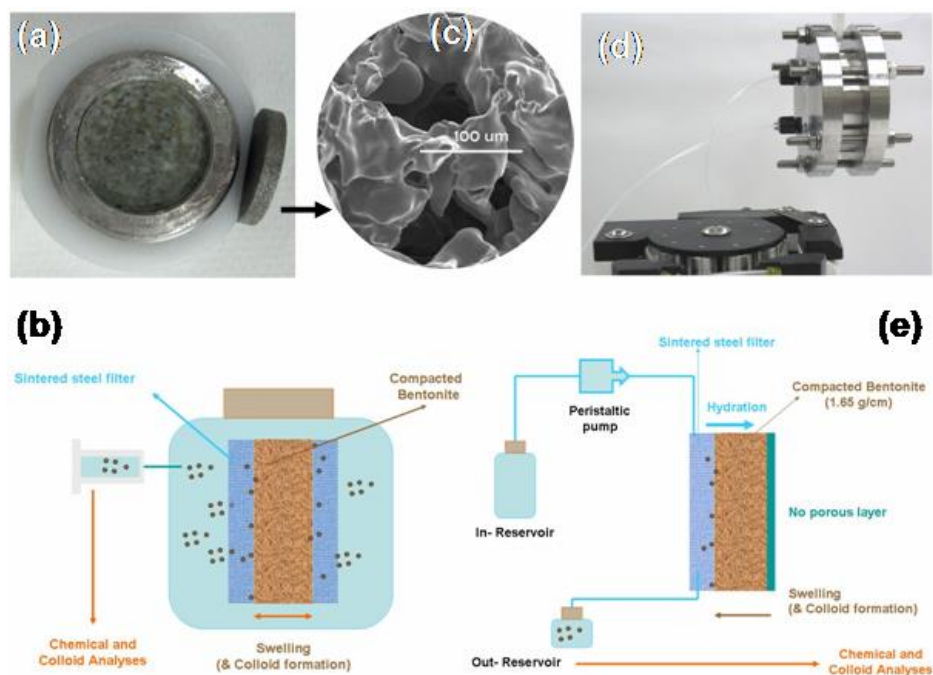


Figure 28: Experimental cells and schematic of the generation tests for static (a and b) or dynamic (d and e) experiments. In (c) a SEM image of the sintered steel porous filter shows large pores.

Provided the porosity of the filters is similar, the filters pore size does not affect appreciably neither the final concentration nor the size of the colloids generated, as shown by Seher et al. (2009) who compared pore sizes of 100, 10 and 2 μm . The experiments under static conditions were performed with *as-received*, Na- and Ca-exchanged clays.

A periodical sampling of the aqueous solution was carried out to analyze the concentration and size of colloids (eventually) formed. One small aliquot of the aqueous solution (approximately 1 mL) was extracted with a syringe after gently shaking the vessel to homogenize the suspension. This allows determining the total mass of clay colloids detached. At the end of the experiment the chemistry of the final solution left was always analyzed, to check by geochemical modeling if dissolution and ionic exchange process occurred.

To determine the generation of colloids under dynamic (flow) conditions and to study the contribution of a water flow on bentonite erosion a different set-up was used. Approximately 46 grams of bentonite compacted to a desired density in cylindrical pellets (5 cm of diameter and 1.24 cm of thickness) are installed in the experimental cell. The cell used for erosion experiments with flow, is similar to that used in through-diffusion experiments (Garcia-Gutierrez et al., 2001), but with one of the two sides closed (Figure 28d). A large reservoir (in-reservoir) contained the initial aqueous solution that entered into the cell through Teflon tubing. The solution was forced through the sintered steel filter with a peristaltic pump and periodically collected after the contact with the bentonite surface, for colloids and chemical analysis (Figure 28e). The water eluted was collected in polyethylene tubes of 20-60 mL for colloid analysis.

The analysis of colloids was performed by Photon Correlation Spectroscopy (PCS) using a Malvern 4700 system equipped with a Spectra - Physics 4W argon laser ($\lambda = 514 \text{ nm}$) and the photomultiplier located at a scattering angle of 90° or a Nano S Malvern apparatus with a He-Ne ($\lambda = 633 \text{ nm}$) with a scattering angle of 173° . PCS was used to determine the size and concentration of colloids in the aqueous solutions as a function of time.

Another set up for erosion experiments under dynamic conditions and the benchmark exercise, consisted on a methacrylate cell, simulating a conductive fracture, shown in Figure 29. In these experiments, apart from the chemical conditions (of water and clay), the velocity of the water at the bentonite surface can be changed and also the dimensions of the artificial fracture.

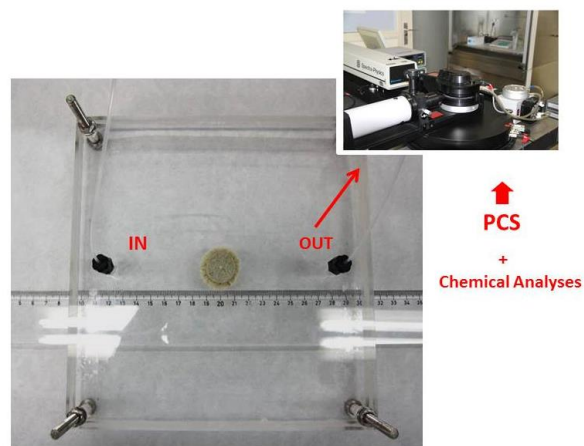


Figure 29: Experimental methacrylate cell simulating a fracture.

The effects of different parameters (density of the clay, the exchange complex of the clay and chemistry of the contacting water) were studied in static experiments. Also a comparison of different raw clays of interest was carried out. Most of the results obtained during the BELBAR Project by CIEMAT have been already described in previous Deliverables. Here, the main results obtained for the main investigated issues focusing on WP1 requirements will be summarized. The main quantitative data will be provided in the Annex of this report.

Mechanisms of erosion of clay particles from the bentonite surface

The static experiments (Figure 28a) were carried out with compacted bentonite confined by porous filters. After hydration, bentonite swells and clay particles are detached from the bentonite surface dispersed and measured in the contact solution.

In these static experiments, the increase of particles in solution is more rapid at the beginning of the erosion process then it slows down and stops. A sort of equilibrium is then reached in closed systems (Deliverable 2.1). The fact that steady-state conditions are reached is a relevant point, because it means that the maximum quantity of colloids generated, will depend on the initial conditions of the system (chemistry of the water, clay, compaction density, etc...), but that the bentonite loss in a static system will not be continuous.

Erosion was also observed in dynamic experiments (with and without fracture). However the dispersion process driven by chemical forces seemed to be more important than the presence of mechanical forces for the overall erosion process (Deliverable 2.2).

Characteristics of the bentonite clays

In static experiments, it has been shown that the compaction density plays a role on the quantity of particle generated from the clay being higher for higher compaction density (Deliverable 2.1). Different experiments were carried out with the FEBEX clay in deionized water in order to understand how the exchange complex may affect erosion. The behavior of the *as-received* FEBEX bentonite was compared with the same clay exchanged in Ca or in Na.

The quantity of colloids generated from the Ca-bentonite was always near or below the PCS experimental detection limit even in low or very low ionic strength solutions. Thus 100 % Ca-bentonites are not expected to be source of colloidal material, due to the high attractive inter-particle forces caused by ion correlation (Kjellander et al, 1988).

On the other hand, the quantity of colloid generated from the *as-received* clay was not very different from that generated by the Na-homoionized clay. The quantity of Na in the exchange complex of the *as-received* FEBEX bentonite (~25 %) is therefore enough to favor almost the maximum possible generation of colloids, at least under favorable conditions in terms of water chemistry. A relatively small amount of Na in the exchange complex may thus significantly increase the dispersivity of the clay as Na adsorbed at the surface dominates the surface properties (Shainberg and Kaiserman, 1969).

A more detailed comparative study of the erosion behaviour of many different raw (and exchanged) bentonites, of interest in the frame of the HLWR concepts of the different participating organisations has been also carried out by CIEMAT. Part of the results has been already described in Deliverable 2.4. More data are presented here.

The erosion behavior of different clay materials and bentonites of different origin was previously studied. A complete physical and geochemical characterization of the bentonites was carried out to gather information for improving the understanding on their erosion behavior depending on the clay characteristics. Different techniques (XRD, FRX, FTIR, TG-DSC, etc.,) were used to evaluate major and minor minerals, clays content, cation exchange capacity, major cations, water content, pore water chemistry, charge distribution and cell formula of the five bentonites. Full details on this characterization can be found elsewhere (Fernandez, 2013). The stability behavior of colloids prepared from the studied clays was also analyzed as a function of the pH and ionic strength (both in raw and Na-exchanged materials) by combining electrophoretic measurements, allowing determining the surface potential of the clay particles (Zetapotential) and Photon Correlation Spectrometry (PCS) as a support of erosion studies.

The clays selected for the experiments were the following:

- (1) Na bentonites like: Wyoming MX-80 bentonite (USA) (Müller-Vonmoss and Kahr, 1983), a Russian bentonite (MSU) from the Khakassia deposit (Sabodina et al., 2006), the commercial Nanocor® Na –bentonite; the B75, a Na activated bentonite from Czech Rockle deposit (Konta, 1986) and Sabenil S65 Czech bentonite, trade name “Sabenil 65”, produced by KERAMOST, Plc., activated.
- (2) Ca-Mg bentonites: FEBEX bentonite from Spain (Huertas et al., 2000); IBECO bentonite from Mylos island in Greece (Koch, 2002; Koch, 2008).
- (3) Fe bentonite: Nontronite Nau-1 a (Clay Minerals Society Source Clays Repository) from the Uley Graphite Mine (South Australia) (Keeling et al., 2000).

The erosion behavior of these materials was compared with the experimental set up described in Figure 28a (Alonso et al., 2007) and using deionized water to maximize erosion. Figure 30 presents the eroded masses obtained from different clays at the compaction density of 1.65g/cm^3 (Nanocor at 1.6g/cm^3) compared to that of the FEBEX bentonite.

The highest eroded mass was measured in the FEBEX clay followed by MX-80, Nanocor. and IBECO. MSU generated lower quantity of particles and almost null erosion was measured from S65, and the nontronite (Nau-1).

In previous works, higher generation was observed from homoionic Na-bentonite than from raw or Ca - homoionic clay (Albarran et al., 2014). In our case, maximum eroded masses determined seems to be more related to the smectite content (higher in the FEBEX case), rather than to the exchangeable Na (higher in Nanocor, Mx-80 or B75 or S65). Figure 31 presents the obtained eroded masses as a function of the clay smectite content. Only Na or Ca-Na bentonites were included, since limited erosion was measured from the Fe-bentonite (Nau-1).

Erosion behavior seems to be more or less related to the clay smectite content, except for the S65 Czech bentonite, that despite being Na- clay with high smectite content did not show appreciable erosion. It is possible that its high Fe-oxide content may be playing a role, inhibiting colloid erosion. Indeed the presence of certain minerals and oxides affects bentonite colloid stability (Mayordomo et al., 2014) and may also affect the clay erosion behavior.

Erosion - 1.65 g/cm³ in Deionised Water

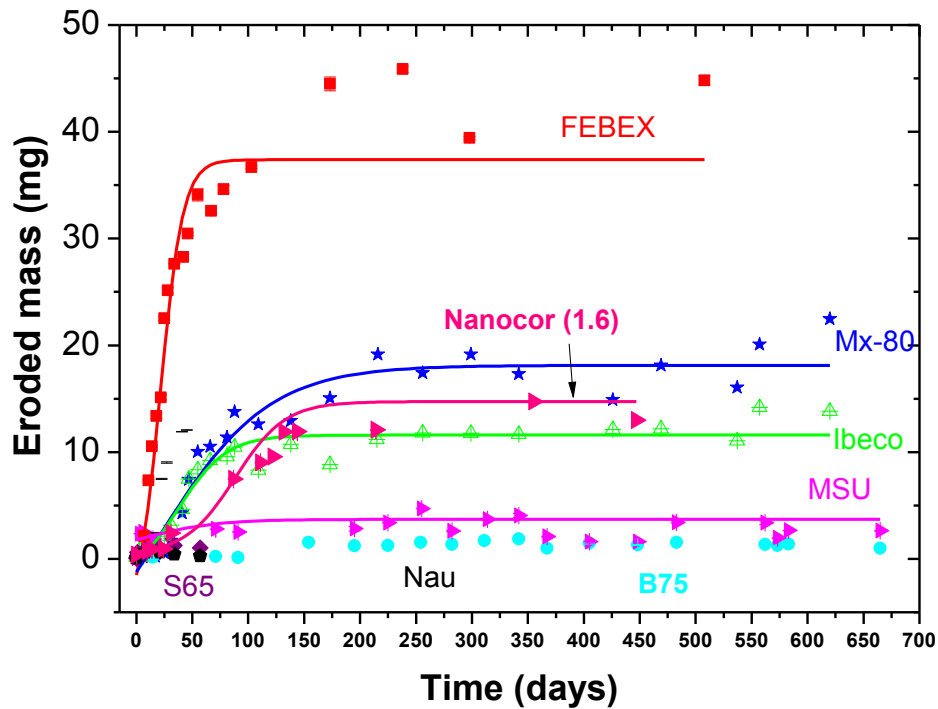


Figure 30. Eroded mass measured, as a function of time, in deionised water from different raw bentonites compacted at 1.65 g/cm³.

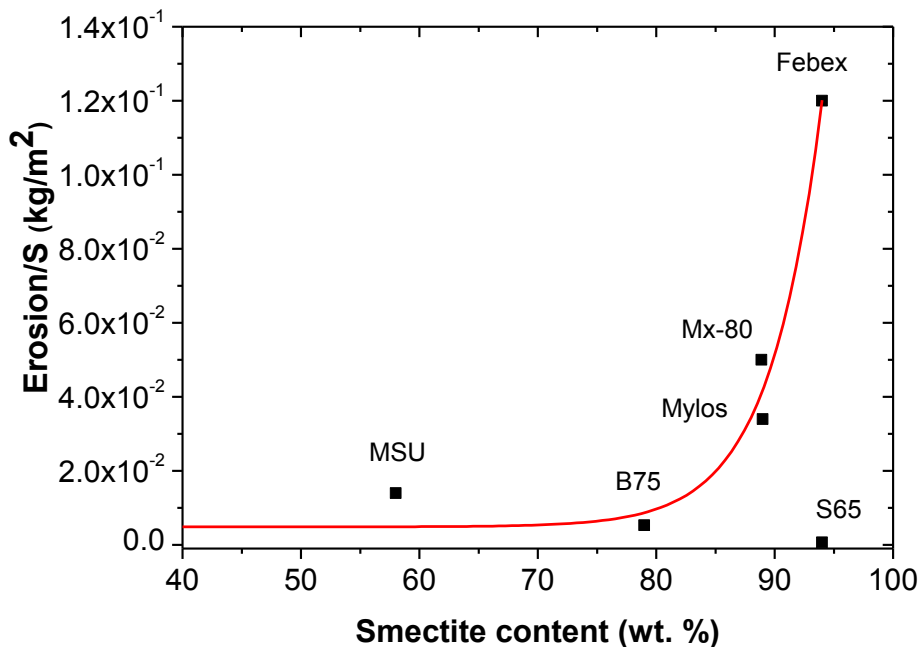


Figure 31. Eroded mass measured in deionised water from different raw bentonites compacted at 1.65 g/cm³ as a function of clay smectite content.

The main differences on the erosion behavior are being also analyzed considering the data on the stability behavior of colloids obtained from the different clays and their physico-chemical characteristics.

Apart from the mentioned bentonites, other clays were also studied, namely: the illite du Puy from France (Gabis, 1958); kaolinite KGa-1-b; "Cheto" SAZ-1 clay from Arizona (USA) and Beidellite SBId-1 from Idaho (USA) provided by the Clay Mineral Society (CMS, USA). Additionally, two saponites were also considered: MCA saponite from Cerro del Aguila (Spain) (Pusch et al., 1996) and B64 saponite. Erosion small or under the detection limit was observed for most of these clays.

Non-swelling materials as kaolinite and illite did not generate colloids, confirming the importance of the smectite presence on overall erosion, but indeed the type of smectite also plays an important role; in fact saponites (and beidellite) did not show appreciable erosion.

Table 1 summarizes the maximum colloidal masses eroded from the compacted bentonites at 1.65 g/cm³. Values are referred to the area available for colloid transport (in this case the two filters surface, 3.54 cm²). The main size of the eroded particles, measured by PCS is also indicated. It is remarkable that when appreciable erosion was measured, the size of the eroded particles was around 300-500 nm, values that are by definition, in the colloidal range (< 1 μm). In the other cases, the particles formed are bigger indicating that stronger forces maintain the clay aggregated inhibiting dispersion.

Table 1: *Maximum masses eroded from bentonites mainly compacted at 1.65 g/cm³ in deionised water, and average particle diameter measured by PCS.*

Bentonite	Colloid/S (Kg/m ²)	Mean size (nm)
FEBEX	$(1.2 \pm 0.5) \cdot 10^{-1}$	338 ± 24
FEBEX (1.6 g/cm ³)	$(6.1 \pm 0.5) \cdot 10^{-1}$	340 ± 20
Nanocor (1.6 g/cm ³)	$(3.5 \pm 0.5) \cdot 10^{-2}$	280 ± 20
Mx-80	$(5 \pm 0.5) \cdot 10^{-2}$	291 ± 31
Ibeco	$(3.4 \pm 0.5) \cdot 10^{-2}$	367 ± 46
MSU	$(1.13 \pm 0.2) \cdot 10^{-2}$	330 ± 140
B75	$(5.4 \pm 0.5) \cdot 10^{-3}$	> 1 μm
Sabenil S65	$(3. \pm 0.5) \cdot 10^{-3}$	≅ 1 μm
Nau-1	$(1.13 \pm 0.5) \cdot 10^{-3}$	> 1 μm

Under the same experimental conditions, the highest quantity of colloidal mass was measured for the FEBEX clay the lowest for the Nau-1 clay. These differences must be related to differences in the clay composition and geochemistry or other characteristics. A more detailed analysis has to be carried out considering all the data reported in Fernandez (2013), especially regarding the charge distribution of the smectite fraction of all the bentonites.

However two points seems to be clear: 1) as far as the Na content in the exchange complex is higher than 20 %, the generation of colloids is not only strongly affected by the exchange

complex; 2) the smectite content may play an important role on natural clay erosion behavior.

To analyze the effect of the presence of clayey materials different from smectite, FEBEX bentonite was mixed with known proportions of illite or kaolinite (50% or 75% weight percent). The experimental set-up and experimental conditions used to evaluate their erosion behavior were totally equivalent to that described for the raw bentonites with compaction density of 1.65 g/cm^3 and deionized water (Deliverable 2.7).

The bentonite mixed with illite or kaolinite exhibited a different erosion behavior. The presence of illite decreases bentonite erosion masses, proportionally to the illite content whereas kaolinite totally inhibited bentonite erosion. This is a quite interesting finding, which probably indicates that the interactions between smectite and illite particles are different from those between smectite and kaolinite. To investigate this effect, stability studies of the mixtures (smectite/illite and smectite/kaolinite) were carried out and the results were presented in Deliverable D4.8

Results obtained on clay mixtures suggests that the presence of other clay minerals or even oxides or other elements affecting bentonite colloid stability may play a major role on decreasing, or even inhibiting, bentonite erosion.

Groundwater chemistry

The ionic strength and composition of the water have been found to be very relevant for the erosion process. In the case of the FEBEX clay, in static tests with: deionized water; natural Grimsel groundwater, GW1, of approx. $1 \cdot 10^{-3} \text{ M}$; $1 \cdot 10^{-3} \text{ M CaCl}_2$ and $1 \cdot 10^{-2} \text{ M NaCl}$; the quantity of colloids generated decreased abruptly when the ionic strength of the solution increased (Figure 32). Ionic strength is not the only parameter affecting the formation and stability of colloids. Divalent ions as Ca are more effective than monovalent ions as coagulants (Shultz-Hardy rule), for this reason is important to analyze the chemical properties of the solution.

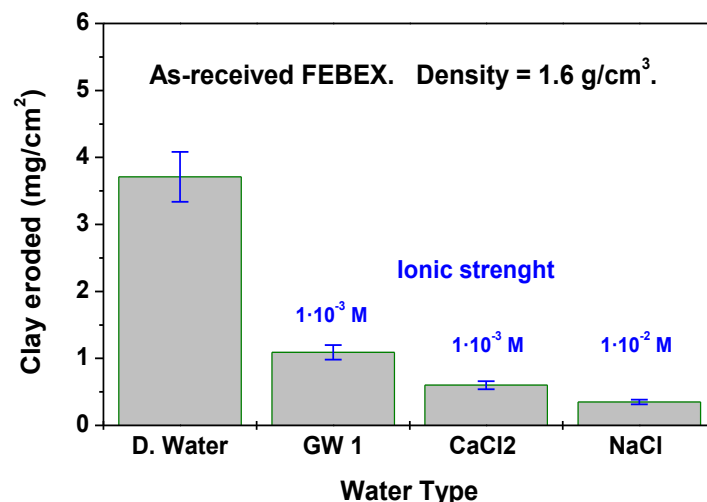


Figure 32: Erosion of the FEBEX clay as a function of the ionic strength of the water.

The important effects of water chemistry on erosion were observed also under dynamic conditions (Deliverable 2.1). At a fixed ionic strength, the presence of Ca in the fresh solutions inhibited the erosion process and the generation of bentonite colloids.

Clay/groundwater interactions

Groundwater evolution, mineral or salt dissolution and cation exchange processes occurring with the clay modify at a long term the chemistry of the clay/groundwater system. The evolution of the chemistry will have an impact on the erosion behavior of the barrier and on the overall mass loss. Experiments with the FEBEX clays showed that Ca is incorporated in the clay and the aqueous solution is therefore depleted in Ca (Deliverable 2.1); this effect has been clearly observed and discussed both in the static and in dynamic generation experiments (Missana et al., 2011). However, major effects on colloid generation are expected only when the surface of the gel becomes saturated in calcium, i.e. when the concentration of Na in the exchange complex of the clay at the gel front has decreased under the critical value limiting its dispersion (Sparks, 2003), as already mentioned. This can occur only in an open system i.e. when fresh water with Ca content is continuously provided as shown in the experiments under dynamic conditions, where the evolution of the concentration of the main ions Cl^- , Ca^{2+} Na^+ and in the water eluted from the generation cell was periodically measured. The ionic exchange effect will be relevant at a long term. Under dynamic conditions, where the contribution of calcium is continuous (even if it is small) the saturation of the bentonite surface in calcium could occur. It has been shown that calcium bentonite does not produce colloids (Kaufhold and Dohrmann, 2008; Missana et al., 2011), thus generation rates are expected to slow down and even stop at a certain time.

Groundwater velocity

The worst scenario in a repository in crystalline rocks is the presence of hydraulically active fractures, for this reason it is important to know if the water flow at the bentonite surface or gel-front may increase colloid detachment and if dependence between the groundwater velocity and erosion rates exists. Figure 33 show erosion tests performed at CIEMAT that lasted more than one year (Deliverable 2.2). In the Figure, the accumulated eroded clay mass is represented as a function of time. First of all, is important to remark that the water chemistry is still critical even under dynamic conditions: in the experiment with NaCl, the quantity of particle generated is significantly higher than in the experiment with NaCl-CaCl₂ mixed electrolyte at the same ionic strength. The second important point is that the erosion rates measured at longer times are much lower than those observed in the initial period, even the water flow was increased (almost one order of magnitude). The erosion rate dependence on the water flow is not evident especially in the less erosive system. Significant changes in colloid erosion rates were not observed, in any case, under successive flow changes and under the experimental conditions analyzed. The system chemistry seems to be much more relevant on colloid erosion rates than flow velocity. It was observed that the continuous calcium supply inhibited colloid erosion. Both findings limit colloid erosion effects on the bentonite barrier integrity. The important effect of ionic exchange on bentonite erosion rates is pointed out. Thus, also under dynamic flow conditions, erosion seems to achieve a maximum possible value, depending on the conditions of the experiments, as was observed in static tests (Alonso et al, 2007; Missana et al, 2011).

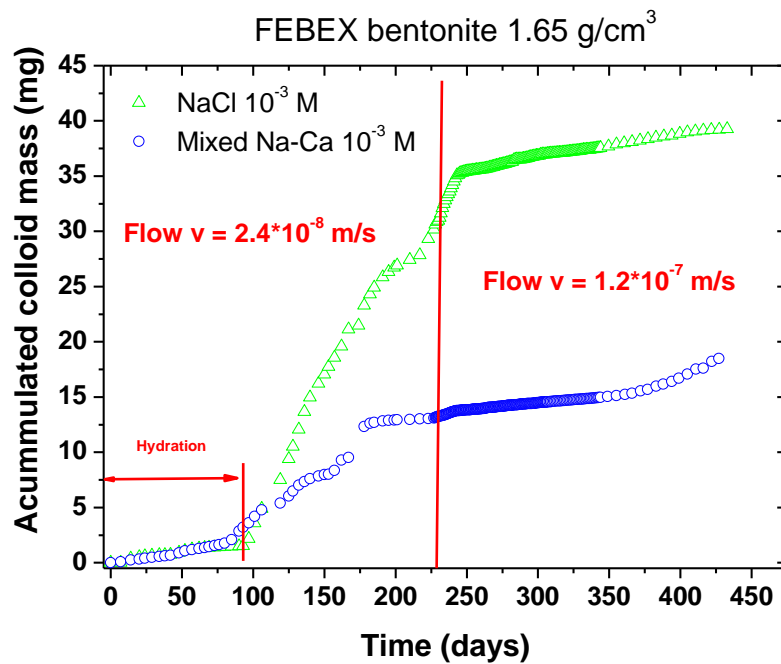


Figure 33. Accumulated colloid mass eroded from FEBEX bentonite in $1 \cdot 10^{-3}$ M NaCl, $1 \cdot 10^{-3}$ M Mixed Na and Ca electrolytes, Initial flow velocity $2.4 \cdot 10^{-8}$ m/s and after 228 days flow velocity changed to $1.2 \cdot 10^{-7}$ M.

The maximum erosion rates measured under different experimental conditions are summarized in Table 2. The values are normalized to the bentonite surface area exposed to water hydration ($19.6 \cdot 10^{-4}$ m²).

Results indicated that, even under flow conditions, there is a maximum threshold of colloid generation of colloids, for given initial conditions, dependent on the characteristics of the gel layer initially formed and on the feasibility of its transport.

Figure 34 (Deliverable 2.2) shows the accumulated masses eroded from two equal cells (C3 and C4) with FEBEX bentonite hydrated with Ca-Na mixed electrolyte ($I=1 \cdot 10^{-3}$ M) in which several consecutive flow changes were carried out. The water velocities varied from $1.5 \cdot 10^{-8}$ to $3.5 \cdot 10^{-6}$ m/s and the experiments lasted more than 3 years.

As can be observed in Figure 34, the behavior is very similar in the two cells, with the tendency of decreasing erosion rate with time, in spite of the different changes in the water velocity. From these results, it seems that the water velocity is less important than chemistry on driving erosion processes, at least considering this range of water flow velocities.

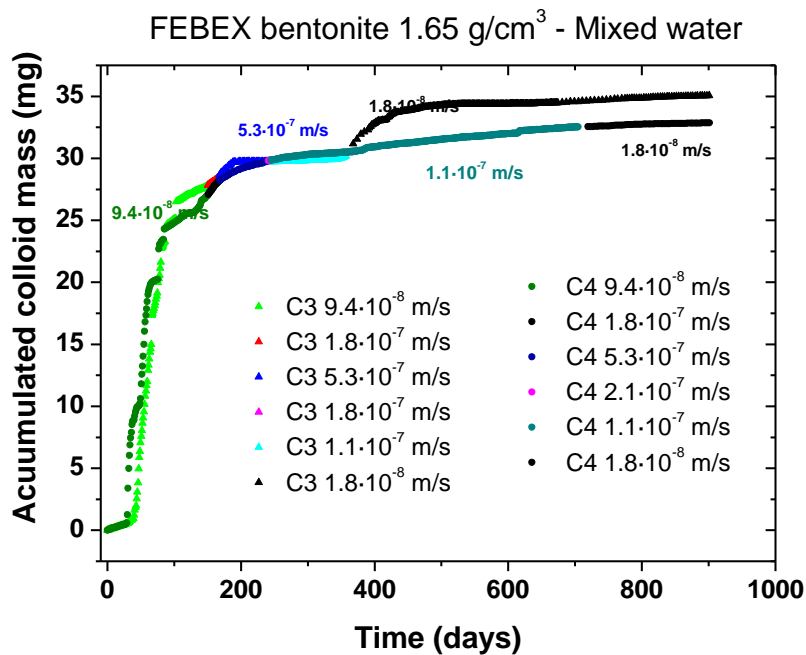


Figure 34. Accumulated colloid mass eroded from FEBEX bentonite in $1 \cdot 10^{-3}$ M Mixed Na and Ca electrolyte, upon consecutive flow velocity changes.

Clay extrusion paths

In static experiments it was observed that the presence of colloids in solution eroded from the clay was limited to the surface available for colloid transport (fracture or porous space) thus, the size of the extrusion paths (joints or fractures) must have a primary importance on the quantity of colloids found in solution. This hypothesis was verified using experimental cells, with the same mass of bentonite, in which one of the two porous filters (Figure 28b) was substituted by a non-porous layer when the extrusion area was halved the concentration of colloid in solution was approximately the half as well. This result indicates the need of normalizing the mass of colloids found in solution to the bentonite surface available for erosion; the advantage of this normalization is that it allows comparing results from different experimental set-up and initial conditions.

Conclusions

Formation of clay particles from compacted and confined bentonite has been analyzed by CIEMAT. The swelling pressure seems to be the first driving force causing the gel intruding the fracture/pores of the rock; thus the density of the clay determines the thickness of the extruded gel layer, potentially subject to erosion. The presence of colloids in solution will be limited to the surface available for colloid transport from the clay surface to the liquid phase and not to the surface available for clay hydration.

In a closed system, a concentration of colloids in equilibrium with the clay surface is reached and dispersion is not continuous. The colloid concentration at the equilibrium depends on

various factors such as clay type, ionic strength and/or Ca content and on the bentonite/water chemical interactions. Chemical conditions are of major importance in all the cases.

Ca-bentonite forms colloids in quantities very near or lower than to the detection limit of our techniques, even in chemical conditions which are favorable for colloid generation. However, a percentage of Na around 20-30 (as that present in FEBEX bentonite) is enough to obtain a generation of colloids similar to that observed for the Na-bentonite.

Results also evidence the importance of water/clay interactions that can be of extreme importance in the evaluation of erosion and stability of colloids in a DGR at a long term.

Different bentonites with different physico-chemical characteristics present different erosion behavior which is mostly related not only to the quantity of the mineral smectite but also to the type of the smectite.

The presence of clayey materials (or oxides) in the bentonite may strongly affect the erosion behavior. If smectite is mixed with illite, the erosion of the system is more or less proportional to the smectite content; on the other hand, the addition of 25 % of kaolinite completely inhibits the erosion of the smectite. This behavior has been related to the stability behavior of the illite/smectite and illite/kaolinite systems.

4) SUMMARY OF MAIN RESULTS FOR WP2 OBTAINED AT KIT-INE

Introduction

Compacted bentonite is considered to be suitable for use as geotechnical barrier in a high level radioactive waste repository in crystalline host rocks. The radionuclides are safely enclosed in the geotechnical barrier if it stays intact, i.e. as long as no water enters the repository. Considering for example the Scandinavian glacial cycles scenario (Bath, 2011; SKB, 2011), melt water may flow down to repository and enter in contact with the compacted bentonite inducing its swelling and a gel formation at the water interface. Accordingly, the bentonite erosion processes and the interaction of the eroded material with radionuclides may play an important role in the safety assessment of a deep radioactive waste repository in crystalline host rock which has to be fully understood (Missana et al., 2003). To simulate erosion processes under dynamic conditions is the aim of this work.

Materials and methods

The experimental set-up used to perform bentonite erosion experiments in this study is adapted from Seher, 2011 (see deliverable 4.2 for details). Raw, Na- and Ca-exchanged MX80 bentonite samples or mixture of both have been compacted in pellets and placed in the double-side reactors. Erosion experiments is conducted by using a synthetic low ionic strength carbonated water to simulate the potential effect of glacial melt water on the bentonite stability (see deliverable 4.2 and Norrfors et al., 2015 for detailed composition).

Results

Samples are regularly taken and analyzed since the beginning of the experiment running now for three years. The results are very reproducible:

- The pH (8.3 ± 0.3) and flow rate (3.0 ± 0.1) $\mu\text{L}\cdot\text{min}^{-1}$ are constant.
- Some material is clearly produced (eroded) and identified as clay according to the concentrations of Si, Al, Mg and Fe recorded. A clear effect of the initial bentonite pellet composition is evidenced.
- The highest erosion is seen in presence of Na-exchanged MX80 pellets while no erosion is observed when using Ca-exchanged ones and it is much more limited when using raw MX80 pellets. When effective, the colloid production presents maxima after ~25 or 50 days to reach a colloid concentration up to ~ 500 mg/L (for Na-exchanged MX80 compacted pellets). Afterwards, the clay colloid concentration is decreasing to level off after 6 months at $\sim < 2$ mg/L.
- These data are used to determine the mass loss rates (MLR) and average mass loss rates (AMLR) under those specific conditions. The results are summarized below (see Table 2).

Table 3: Results of the dynamic erosion experiment performed in double-sided reactors

Type of Test						
	2.5 years		Swelling observed: 30 % solution retained over the three first days			
Dynamic conditions (time)	907	907	907	907		days
Flow	(3.0 ± 0.1) µL / min 2.3 10-4 m/s	(3.0 ± 0.1) µL / min 2.3 10-4 m/s	(3.0 ± 0.1) µL / min 2.3 10-4 m/s	(3.0 ± 0.1) µL / min 2.3 10-4 m/s		m/s
No flow	no	no	no	no		
Confined	yes	yes	yes	yes		YES/NO
Free Swelling	no	no	no	no		YES/NO
Sloped	no	no	no	no		Angle
Fracture dimensions			SS Porous filter: 20 µm; Surface area: 2.86 cm ² ; porosity 29.4%, frit volume 134.7 µL, real surface contact area: 0.842 cm ²			cm ²
Results	Raw MX80	Na-MX80	Ca-MX80	Na-Ca-MX80		
Test duration	21768	21768	21768	21768		hours
Extrusion Distance (Filter Thickness)	0.16	0.16	0.16	0.16		cm
Mass loss	0,046 ± 0,006	0,90 ± 0,2	none	0,33 ± 0,07		Kg/m ²
Mass Loss/initial mass	0,08 ± 0,01	1,74 ± 0,09	none	0,6 ± 0,1		%
Mass Eluted (colloids)	3,83 ± 0,54	75,5 ± 1,7	none	28,0 ± 6,0		mg
Mass loss rate (MLR)	0.051 ± 0,007	1.01 ± 0,02	none	0,37 ± 0,08		Kg/(y·m ²)
Time used for MLR calculations	7800	7800	none	7800		hours
Average mass loss rate (AMLR)	0,026 ± 0,005	0,37 ± 0,01	none	0,15 ± 0,03		Kg/(y·m ²)
Time used for AMLR calculations	21768	21768	none	21768		hours
Size of colloids	162 ± 32	131 ± 3	none	132 ± 7		nm
Methodology	PCS	PCS	-	PCS		
Does erosion stop (qualitative)?	plateau	plateau	YES:NO erosion detected	plateau		YES/NO

- Interestingly, in agreement with literature data and other works (Norrfors et al., 2015), instant releases of sodium, sulphate and chloride are clearly evidenced and attributed to the dissolution of accessory minerals present in the raw bentonite (like gypsum or halide) followed by cationic exchange process.
- The size of the eroded material collected after ~ 1 month was determined by PCS. The intensity-weighted hydrodynamic diameters recorded for the clay colloids eroded are 162 ± 32 nm from the raw-MX80 pellets, 131 ± 3 nm from the Na-exchanged MX80 pellets and 132 ± 7 nm from the mixed Na-Ca-exchanged MX80 pellets. They agree with the sizes already previously reported for clay colloids extracted by centrifugation (Missana et al., 2003; Bouby et al. 2011; Norrfors et al., 2015).
- A Cs, Eu and U sorption test was performed with the eroded material. Cs is not sorbed. No U sorption can be demonstrated which agrees with our latest results (Norrfors et al., 2016). As only a partial removal of the clay colloids was possible in this single test (centrifugation at 16192 x g), one can only state that a minimum of 20 % up to 40 % of Eu is sorbed under the present conditions, with apparently a lower sorption on the eroded material obtained from the raw MX80 pellets. Further work is in progress to obtain a more precise Eu sorption quantification.

REFERENCES

- Albarran, N. et al., 2014. Size distribution analysis of colloid generated from compacted bentonite in low ionic strength aqueous solutions. *Applied Clay Science*, 95: 284–293.
- Alonso, U., Missana, T. and Garcia-Gutierrez, M., 2007. Experimental approach to study the colloid generation from the bentonite barrier to quantify the source term and to assess its relevance on the radionuclide migration, *Scientific Basis for Nuclear Waste Management XXX*. Materials Research Society Symposium Proceedings, pp. 605-610.
- Bath, A., 2011. Infiltration of dilute groundwaters and resulting groundwater compositions at repository depth. Swedish Radiation Safety Authority.
- Birgersson M., Börgesson L., Hedström M., Karnland O., Nilsson U. (2009). Bentonite erosion – Final report. SKB Technical Report, TR-09-34, SKB Stockholm.
- Birgersson M., Karnland O. (2009). Ion equilibrium between montmorillonite interlayer space and external solution –consequences for diffusional transport. *Geochim. Cosmochim. Acta* 73, 1908-1923.
- Bouby, M.; Geckeis, H.; Lützenkirchen, J.; Mihai, S.; Schäfer, T. (2011) Interaction of bentonite colloids with Cs, Eu, Th and U in presence of humic acid: a Flow Field-Flow Fractionation study. *GCA*, 75, 3866-3880.
- Fernandez, A.M., 2013. Mineralogical, geochemical and pore water characterization of different bentonites in the context of the BELBAR project. CIEMAT Report June 2013, 40 pp. Madrid (Spain).
- Gabis, V., 1958. Etude préliminaire des argiles oligocènes du Puy-en-Velay (Haute-Loire). *Bull. Soc. Franc. Minéral. Cristallog.*, 81: 183-185.
- García-Gutiérrez M, Missana T., Mingarro M., Samper J., Dai Z., Molinero J. (2001). Solute transport properties of compacted Ca bentonite used in the FEBEX Project. *Journal of Contaminant Hydrology*, 47(2-4), 127-137.
- Hedström M., Birgersson M., Nilsson U., Karnland O. (2011) Role of cation mixing in the sol formation of Ca/Na-montmorillonite. *Phys. Chem. Earth* 36, 1564-1571.
- Hedström M., Karnland O. (2012). Donnan equilibrium in Na-montmorillonite from a molecular dynamics perspective. *Geochim. Cosmochim. Acta* 77, 266-274.
- Hsiao, Y.-W., Hedström, M., 2015. Molecular Dynamics Simulations of NaCl Permeation in Bihydrated Montmorillonite Interlayer Nanopores. *J. Phys. Chem. C* 119, 17352–17361.
- Huber, F.M. et al., 2015. Radionuclide desorption kinetics on synthetic Zn/Ni-labeled montmorillonite nanoparticles. *Geochimica et Cosmochimica Acta*, 148: 426–441.
- Huertas, F. et al., 2000. Full scale engineered barriers experiment for a deep geological repository for high-level radioactive waste in crystalline host rock. EC Final REPORT EUR 19147, EC Final REPORT EUR 19147.
- Karnland O., Olsson S., Nilsson U. (2006). Mineralogy and Sealing Properties of Various Bentonites and Smectite-rich Clay Material. SKB Technical Report, TR-06-30, SKB Stockholm.
- Kaufhold S. and Dohrmann R. (2008), Detachment of colloidal particles from bentonites in water, *Applied Clay Science*, 39, 50-59.
- Keeling, J.L., Raven, M.D. and Gates, W.P., 2000. Geology and characterization of low hydrothermal nontronites from weathered metamorphic rocks at the Uley graphite mine, south Australia. *Clays and Clay Minerals*, 48(5): 537-548.
- Kjellander R., Marcelja S., Quirk J., 1988. Attractive double Layer Interactions between Calcium and Clay particles, *JCIS*, 126, 194-211.
- Koch, D., 2002. Bentonites as a basic material for technical base liners and site encapsulation cut-off walls. *Applied Clay Science*, 21(1-2): 1-11.

- Koch, D., 2008. European Bentonites as alternatives to MX-80. *Science & Technology Series*, 334: 23-30.
- Konta, J., 1986. Textural variation and composition of bentonite derived from basaltic ash. *Clays and Clay Minerals*, 34(3): 257-265.
- Marcke, P.V. and Laenen, B., 2005. The Ypresian Clays as Possible Host Rock for Radioactive Waste Disposal: An Evaluation. NIROND TR.2005-01 Report (Belgium).
- Mayordomo, N., Alonso, U., Missana, T., Benedicto, A. and García-Gutiérrez, M., 2014. Addition of Al₂O₃ nanoparticles to bentonite: effects on surface charge and Cd sorption properties., *Scientific Basis For Nuclear Waste Management XXXVII. Mat. Res. Symp. Proc.*, pp. 131-138.
- Missana, T., Alonso, U., Albarran, N., Garcia-Gutierrez, M. and Cormenzana, J.-L., 2011. Analysis of colloids erosion from the bentonite barrier of a high level radioactive waste repository and implications in safety assessment. *Physics and Chemistry of the Earth*, 36(17-18): 1607-1615.
- Missana, T., Alonso, U., Turrero, M.J., 2003. Generation and stability of bentonite colloids at the bentonite/granite interface of a deep geological radioactive waste repository. *J. Cont. Hydrol.*, 61, 17-31.
- Müller-Vonmoss, M. and Kahr, G., 1983. Mineralogische Untersuchungen von Wyoming Bentonite MX-80 und Montigel. NTB 83-13, Nagra, Wettingen, Switzerland.
- Norrfors, K.K., Bouby, M., Heck, S., Finck, N., Marsac, R., Schäfer, T., Geckeis, H., Wold, S. (2015) Montmorillonite colloids: I. Characterization and stability of dispersions with different size fractions. *Applied Clay Science*, 114, pp. 179-189.
- Norrfors, K.K., Marsac, R., Bouby, M., Heck, S., Wold, S., J. Lützenkirchen, J.; Schäfer, T., (2016) Montmorillonite colloids: II. Colloidal Size Dependency on Radionuclide Adsorption, under Revision, *Applied Clay Science*.
- Pusch, R., Karnland, O. and Sanden, T., 1996. Final Report of Physical Test program concerning spanish clays (saponites and bentonites). ENRESA Report 02/96, (Spain).
- Sabodina, M.N., Kalmykov, S.N., A., A.e.K., V., Z.E. and A., S.Y., 2006. Behavior of Cs, Np(V), Pu(IV), and U(VI) in Pore Water of Bentonite. *Radiochemistry*, 48(5): 488 - 492.
- Schatz T, Kanerva N, Martikainen J, Sane P, Olin M, Seppälä A, Koskinen K, (2013). Buffer erosion in dilute groundwater. POSIVA 2012-44. Posiva Oy, Olkiluoto, Finland.
- Seher H., Albarran N., Hauser W., Götz R., Missana T., Geckeis H., Fanghänel T., Schäfer T. (2009) Colloid generation by erosion of compacted bentonite under different geochemical conditions, 4th FUNMIG Annual Workshop Proceedings, FZK Report FZKA 7461, pag. 139-145, FZK Karlsruhe, Germany.
- Seher, 2011: Influence of colloids on the migration of radionuclides, PhD thesis, University of Heidelberg, Faculty of Chemistry and Earth Sciences.
- Shainberg, I., Kaiserman, A. (1969). Kinetics of the formation and breakdown of Ca-montmorillonite tactoids. *Soil Sci. Soc. Am. Proc.* 33, 547-551.
- SKB, 2011. Long-Term Safety for the Final Repository for Spent Nuclear Fuel at Forsmark, Main Report of the SR-Site Project. SKB technical report TR -11-01. Svensk Kärnbränslehantering AB.
- Sparks D.L. (2003) *Environmental Soil Chemistry*, Academic Press, Elsevier (USA), 352 p.



EUROPEAN
COMMISSION

Community research

ANNEX

BELBaR





EUROPEAN
COMMISSION

Community research

B+TECH

BELBaR



#50	Type of Test:	artificial fracture test	notes																
	aperture size	1	mm	smooth, planar fracture															
	Stagnant conditions (time)	n/a	days																
	Flow	5.79E-06	m/s																
	No flow	n/a																	
	Confined	n/a	YES/NO																
	Free Swelling	n/a	YES/NO																
	Sloped	0°	Angle	horizontal fracture															
	Fracture dimensions	576	cm ²	24 cm × 24 cm fracture plane															
	Results			notes															
	Test Duration	651	hours																
	Extrusion Distance	4.48	cm	average distance over last 170 h of test; corresponds to radial increase of the extruding front from the sample center															
	Eroding Surface Area	2.81E-04	m ²																
	Mass Loss	14.0	Kg/m ²																
	Mass Loss/Initial Mass	38	%																
	Mass Eluted (colloids)	n/d	mg																
	Mass loss rate (MLR)	n/a	Kg/(y·m ²)																
	Time used for MLR calculations	n/a	hours																
	Average mass loss rate (AMLR)	188	Kg/(y·m ²)																
	Time used for AMLR calculations	651	hours																
	Size of colloids	n/d	nm																
	Methodology	post-mortem gravimetric		both remaining sample mass and extruded mass are determined from post-mortem analyses; lost mass is calculated as initial sample mass - (remaining sample mass + extruded mass)															
	Does erosion stop (qualitative)?	no	YES/NO																
	COMMENTS																		
	(*)																		
	n/d = not determined																		
	n/a = not applicable																		

CLAY TECHNOLOGY AB

BELBaR

DELIVERABLE 2.12: WP2 partners final report on bentonite erosion

Dissemination level: PU

Date of issue of this report: 31/12/15

Claytech#2				
	ORGANISATION: Clay Technology AB			
	Bentonite Type: Smectite fraction MX80			
	Pre - conditioning ?	Homoionization Na & Ca		
	Mass		g	
	Dry Density	1.26	g/cm ³	
	Na in Exch. Compl.	50	%	
	Ca in Exch. Compl.	50	%	
	Solution: "Grimsel" simulant			
		INITIAL		FINAL
	Ionic Strength	1.12	mM	
	pH			
	Conductivity		uS/cm	
	Divalent ions concentration	0.14	mM	
	Volume		mL	
	Type of Test	radial swelling *		
	Stagnant conditions (time)		days	
	Flow	6.90E-05	m/s	
	No flow			
	Confined		YES/NO	
	Free Swelling	YES	YES/NO	
	Sloped	45	Angle	
	Fracture aperture	120	µm	
	Results			
	Test duration	24	hours	
	Extrusion Distance	0.9	cm	
	Mass loss	0.650	Kg/m ²	
	Mass Loss/initial mass		%	
	Mass Eluted (colloids)	12.7	mg	
	Mass loss rate (MLR)	240	Kg/(y·m ²)	
	Time used for MLR calculations	24	hours	
	Average mass loss rate (AMLR)	not applicable	Kg/(y·m ²)	
	Time used for AMLR calculations	not applicable	hours	
	Size of colloids		nm	
	Methodology			
	Does erosion stop (qualitative)?	NO	YES/NO	
COMMENTS	(*) Radial swelling into 120 µm fracture. Initial diameter = 35 mm.			

CIEMAT

BELBaR

DELIVERABLE 2.12: WP2 partners final report on bentonite erosion

Dissemination level: PU

Date of issue of this report: 31/12/15

CIEMAT #02 REV				
ORGANISATION: CIEMAT				
Bentonite Type: FEBEX		Main exchangeable cation		
Pre - conditioning ?	Na- homionic	Ca-homionic		
Mass	4.72	4.72	g	
Dry Density	1.6	1.6	g/cm ³	
Na in Exch. Compl.	~100	0	%	
Ca/Mg in Exch.Compl.	0	~100 Ca	%	
Solution: Deionised water				
	INITIAL			FINAL
Ionic Strength	0.01	0.01	mM	0.5-1
pH	6.3	6.3		6.5/6.5
Conductivity	8	8	uS/cm	262/70
Divalent ions concentration	0	0	mM	
Volume	200	200	mL	
Type of Test				
Aperture size	n/a	n/a	mm	
Stagnant conditions (time)	100	100	days	
Flow	NO	NO	m/s	
No flow	X	X		
Confined	YES	YES	YES/NO	
Free Swelling	NO	NO	YES/NO	
Sloped	NO	NO	Angle	
Fracture dimensions	3.53	3.53	cm ²	* 2x available surfaces. Filter porosity (60%) not corrected.
Results				
Test duration	100	100	days	
Extrusion Distance	0.31	0.31	cm	* Filter thickness
Eroding surface area	3.53E-04	3.53E-04	m ²	* 2x available surfaces. Filter porosity (60%) not corrected.
Mass loss	0.073	0.001	Kg/m ²	
Mass Loss/initial mass	0.55	0.01	%	
Mass Eluted (colloids)	25.8	0.39	mg	
Mass loss rate (MLR)	1.30E-01	5.17E-03	Kg/(y·m ²)	Initial slope (*)
Time used for MLR calculations	100	100	days	Until equilibrium (*)
Average mass loss rate (AMLR)	n/a	n/a	Kg/(y·m ²)	
Time used for AMLR calculations	n/a	n/a	hours	
Size of colloids	420	> 1000 nm	nm	
Methodology				
Does erosion stop (qualitative)?	YES	YES	YES/NO	
COMMENTS				

CIEMAT #03 REV						
ORGANISATION: CIEMAT						
Bentonite Type: FEBEX		Natural Groundwaters				
Pre - conditioning ?	Raw	Raw				
Mass	4.86	4.86	g			
Dry Density	1.65	1.65	g/cm ³			
Na in Exch. Compl.	28.2	28.2	%			
Ca/Mg in Exch. Compl.	34.9//35.14	34.9//35.14	%			
Solution: Grimse! (GW)		Aspö (AW)				
	INITIAL	INITIAL		Final GW	Final AW	
Ionic Strength	1	20	mM	1	200	
pH	8.7	6.6		6.7	7.2	
Conductivity	100	1371	uS/cm	100	1380	
Divalent ions concentration	0.2	20	mM			
Volume	200	200	mL			
Type of Test						
Aperture size	n/a	n/a	mm			
Stagnant conditions (time)	100	100	days			
Flow	NO	NO	m/s			
No flow	X	X				
Confined	YES	YES	YES/NO			
Free Swelling	NO	NO	YES/NO			
Sloped	NO	NO	Angle			
Fracture dimensions	3.53	3.53	cm ²	* 2x available surfaces. Filter porosity (60%) not corrected.		
Results						
Test duration	255	300	days			
Extrusion Distance	0.31	0.31	cm	* Filter thickness		
Eroding surface area	3.53E-04	3.53E-04	m ²	* 2x available surfaces. Filter porosity (60%) not corrected.		
Mass loss	0.053	0.000	Kg/m ²			
Mass Loss/initial mass	0.4	0.00	%			
Mass Eluted (colloids)	18.84	0.13	mg			
Mass loss rate (MLR)	1.55E-01	1.00E-04	Kg/(y·m ²)	Initial slope	(*)	
Time used for MLR calculations	75	300	days	Until equilibrium	(*)	
Average mass loss rate (AMLR)	n/a	n/a	Kg/(y·m ²)			
Time used for AMLR calculations	n/a	n/a	hours			
Size of colloids	350	> 1000 nm	nm			
Methodology						
Does erosion stop (qualitative)?	YES	YES	YES/NO			
COMMENTS						
(*) Equilibrium concentration of colloid is reached at long times. The time used for MLR calculation is from the starting of the experiment to the moment in which the equilibrium is reached						

CIEMAT #04 REV																						
	ORGANISATION:	CIEMAT	Clay minerals																			
	Bentonite Type:	Mx-80	Mylos	B75 - CzR	MSU- Russia																	
	Pre - conditioning ?	Raw	Raw	Raw	Raw																	
	Mass	4.387	4.649	4.398	4.798					g												
	Dry Density	1.65	1.65	1.65	1.65					g/cm ³												
	Na in Exch. Compl.	57.5	27.23	37.03	77.7					%												
	Ca/Mg in Exch.Compl.	18.41//7.07	34.2//30.92	36.5//22.38	1.10//4.22					%												
	Solution:	Deionised water																				
		INITIAL									FINAL											
	Ionic Strenght	0.01	0.01	0.01	0.01					mM												
	pH	6.3	6.3	6.3	6.3						8.9/9.3/9.3/9.9											
	Conductivity	8	8	8	8					uS/cm	360/290/680/390											
	Divalent ions concentration	0	0	0	0					mM												
	Volume	200	200	200	200					mL												
	Type of Test																					
	Aperture size	n/a	n/a	n/a	n/a					mm												
	Stagnant conditions (time)	100	100	100	100					days												
	Flow	NO	NO	NO	NO					m/s												
	No flow	X	X	X	X																	
	Confined	YES	YES	YES	YES					YES/NO												
	Free Swelling	NO	NO	NO	NO					YES/NO												
	Sloped	NO	NO	NO	NO					Angle												
	Fracture dimensions	3.53	3.53	3.53	3.53					cm2	* 2x available surfaces. Filter porosity (60%) not corrected.											
	Results																					
	Test duration	620	620	620	400					days												
	Extrusion Distance	0.31	0.31	0.31	0.31					cm	* Filter thickness											
	Eroding surface area	3.53E-04	3.53E-04	3.53E-04	3.53E-04					m2	* 2x available surfaces. Filter porosity (60%) not corrected.											
	Mass loss	0.052	0.040	0.005	0.011					Kg/m ²												
	Mass Loss/initial mass	0.42	0.30	0.04	0.08					%												
	Mass Eluted (colloids)	18.3	14	1.9	4					mg												
	Mass loss rate (MLR)	1.76E-01	1.76E-01	1.55E-03	1.80E-02					Kg/(y·m ²)	Initial slope (*)											
	Time used for MLR calculations	100	100	600	100					days	Until equilibrium (*)											
	Average mass loss rate (AMLR)	not applicable	not applicable	not applicable	not applicable					Kg/(y·m ²)												
	Time used for AMLR calculations	not applicable	not applicable	not applicable	not applicable					hours												
	Size of colloids	280	380	286	350					nm												
	Methodology	PCS	PCS	PCS	PCS																	
	Does erosion stop (qualitative)?	YES	YES	YES	YES					YES/NO												
	COMMENTS																					
		(*) Equilibrium concentration of colloid is reached at long times. The time used for MLR calculation is from the starting of the experiment to the moment in which the equilibrium is reached																				

KIT INE

BELBaR

DELIVERABLE 2.12: WP2 partners final report on bentonite erosion

Dissemination level: PU

Date of issue of this report: 31/12/15

ORGANISATION: CIEMAT				ORGANISATION: KIT-INE				ORGANISATION: KIT-INE				
Bentonite Type: FEBEK				Bentonite Type: FEBEK				Bentonite Type: FEBEK				
Pre-conditioning ?	Homologization in Na			Pre-conditioning ?	Homologization in Na			Pre-conditioning ?	Homologization in Ca			Mixture
Mass	4.72	g		Mass	4,90 and 4,88	g		Mass	4,90 and 4,89	g		4,80 and 4,81
Dry Density	1.6	g/cm ³		Dry Density	1.6	g/cm ³		Dry Density	1.6	g/cm ³		1.6
Na in Exch. Compl.	100	%		Na or Ca in Exch. Compl.	-	%		Na or Ca in Exch. Compl.	100	%		100
Ca/Mg in Exch. Compl.		%		Ca/Mg in Exch. Compl.	-	%		Ca/Mg in Exch. Compl.	50	%		50
Solution: Grimsel water				Solution: SGW *				Solution: SGW *				
Ionic Strength	1	mM	FINAL	Ionic Strength	1.6	mM	FINAL	Ionic Strength	1.6	mM	FINAL	1.6
pH	7.9		7.67	pH	8.3 ± 0.3		8.3 ± 0.3	pH	8.3 ± 0.3		8.3 ± 0.3	8.3 ± 0.3
Conductivity	130	uS/cm	157	Conductivity	n.d.	uS/cm	n.d.	Conductivity	n.d.	uS/cm	n.d.	8.3 ± 0.3
Divalent ions concentration	0.2	mM		Divalent ions concentration	see SGW composition above	mM		Divalent ions concentration	see SGW composition above	mM		n.d.
Volume	200	mL		Volume	11,6 mL (in the reactor)	mL		Volume	11,6 mL (in the reactor)	mL		11,6 mL (in the reactor)
Type of Test				Type of Test				Type of Test				
Stagnant conditions (time)	255	days		Stagnant conditions (time)	907	days		Stagnant conditions (time)	907	days		907
Flow	NO	m/s		Flow	NO	m/s		Flow	NO	m/s		NO
No flow	X			No flow	NO			No flow	NO			NO
Confined	YES	YES/NO		Confined	YES	YES/NO		Confined	YES	YES/NO		YES
Free Swelling	NO	YES/NO		Free Swelling	NO	YES/NO		Free Swelling	NO	YES/NO		NO
Sloped	NO	Angle		Sloped	NO	Angle		Sloped	NO	Angle		NO
Fracture dimensions				Fracture dimensions				Fracture dimensions				
Results	3.53	cm ²	Porous Filter	Results	Raw MX80	Na-MX80	Ca-MX80	Results	Raw MX80	Na-MX80	Ca-MX80	Na-Ca-MX80
Test duration	6120	hours		Test duration	21768	21768	21768	Test duration	21768	21768	21768	21768
Extrusion Distance	0.31	cm	Filter thickness	Extrusion Distance (Filter Thickness)	0.16	0.16	0.16	Extrusion Distance (Filter Thickness)	0.16	0.16	0.16	0.16
Mass loss	0.053	Kg/m ²		Mass loss	0,046 ± 0,006	0,90 ± 0,2	none	Mass loss	0,046 ± 0,006	0,90 ± 0,2	none	0,33 ± 0,07
Mass Loss/initial mass	0.4	%		Mass Loss/initial mass	0,08 ± 0,01	1,74 ± 0,09	none	Mass Loss/initial mass	0,08 ± 0,01	1,74 ± 0,09	none	0,6 ± 0,1
Mass Eluted (colloids)	18.84	mg		Mass Eluted (colloids)	3,83 ± 0,54	75,5 ± 1,7	none	Mass Eluted (colloids)	3,83 ± 0,54	75,5 ± 1,7	none	28,0 ± 6,0
Mass loss rate (MLR)	600777 0.5 instead???	Kg/(y·m ²)	Initial (*)	Mass loss rate (MLR)	0,051 ± 0,007	1,01 ± 0,02	none	Mass loss rate (MLR)	0,051 ± 0,007	1,01 ± 0,02	none	0,37 ± 0,08
Time used for MLR calculations	768	hours	Initial (*)	Time used for MLR calculations	7800	7800	none	Time used for MLR calculations	7800	7800	none	7800
Average mass loss rate (AMLR)	not applicable	Kg/(y·m ²)		Average mass loss rate (AMLR)	0,026 ± 0,005	0,37 ± 0,01	none	Average mass loss rate (AMLR)	0,026 ± 0,005	0,37 ± 0,01	none	0,15 ± 0,03
Time used for AMLR calculations	not applicable	hours		Time used for AMLR calculations	21768	21768	none	Time used for AMLR calculations	21768	21768	none	21768
Size of colloids	350	nm		Size of colloids	162 ± 32	131 ± 3	none	Size of colloids	162 ± 32	131 ± 3	none	132 ± 7
Methodology	PCS			Methodology	PCS	PCS		Methodology	PCS	PCS		PCS
Does erosion stop (qualitative)?	YES	YES/NO		Does erosion stop (qualitative)?	plateau	plateau	YES:NO erosion detected	Does erosion stop (qualitative)?	plateau	plateau	YES:NO erosion detected	plateau
COMMENTS				COMMENTS				COMMENTS				
didn't you consider the porosity of your filter ?? 40% isn't it? So 1.41 cm ² instead of 3.53...we will have then much more comparable results for the Na-exc-MX80 system :-)				The erosion seems to be greatly increased under dynamic flow conditions compared to stagnant ones				The erosion seems to be greatly increased under dynamic flow conditions compared to stagnant ones				
(*) Equilibrium concentration of colloid is reached at long times. The time used for MLR calculation is from the starting of the experiment to the moment in which the equilibrium is reached				*SGW : synthetic carbonated groundwater [Na ⁺] = 1.2 mM, [Ca ²⁺] = 0.05 mM, [F ⁻] = 0.1 mM, [Cl ⁻] = 0.074 mM, [SO ₄ ²⁻] = 0.04 mM and [HCO ₃ ⁻] = 1.0 mM. IS = 1.6 mM, pH = 8.4 ± 0.1 and E _{h(25°C)} = +0.35 ± 0.05 V				n.d. : not determined				
Mass loss rate with 1.41 cm ²	0.1336	Kg/m ²										
Mass loss rate (MLR)	1.52	Kg/(y·m ²)										
Time used for MLR calculation	768	hours										

BELBaR

DELIVERABLE 2.12: WP2 partners final report on bentonite erosion

Dissemination level: PU

Date of issue of this report: 31/12/15